Impact of x-ray dose on track formation and data analysis for CR-39-based proton diagnostics

H.G. Rinderknecht,[1, a)] J. Rojas-Herrera,[1] A.B. Zylstra,[1, b)] J.A. Frenje,[1] M. Gatu Johnson,[1] H. Sio,[1] N. Sinenian,[1] M.J. Rosenberg,[1, c)] C.K. Li,[1] F.H. Séguin,[1] R.D. Petrasso,[1] T. Filkins,[2] Jeffrey A. Steidle,[3] Jessica A. Steidle,[2] N. Traynor,[2] and C. Freeman[2]

[1)] *Massachusetts Institute of Technology, Cambridge, Massachusetts 02139 USA*
[2)] *State University of New York at Geneseo, Geneseo, New York 14454*
[3)] *Rochester Institute of Technology, Rochester, New York 14623*

The nuclear track detector CR-39 is used extensively for charged particle diagnosis, in particular proton spectroscopy, at Inertial Confinement Fusion (ICF) facilities. These detectors can absorb x-ray doses from the experiments on the order of 1–100 Gy, the effects of which are not accounted for in the previous detector calibrations. X-ray dose absorbed in the CR-39 has previously been shown to affect the track size of alpha particles in the detector, due primarily to a measured reduction in the material bulk etch rate [J. Rojas-Herrera, et al. RSI 86, 033501 (2015)]. Similarly to the previous findings for alpha particles, protons with energies in the range 0.5–9.1 MeV are shown to produce tracks that are systematically smaller as a function of the absorbed x-ray dose in the CR-39. The reduction of track size due to x-ray dose is found to diminish with time between exposure and etching if the CR-39 is stored at ambient temperature, and complete recovery is observed after two weeks. The impact of this effect on the analysis of data from existing CR-39-based proton diagnostics on OMEGA and the National Ignition Facility (NIF) is evaluated and best practices are proposed for cases in which the effect of x rays is significant.

I. INTRODUCTION

Nuclear diagnostics provide valuable and unique experimental data in the context of high energy density (HED) plasmas and inertial confinement fusion (ICF). Spectroscopy of neutrons and charged particles produced by light-ion fusion reactions in ICF implosions is used to infer the temperature and areal density (ρR) of the compressed fuel,[1–3] two key metrics of the success of the implosion.[4] Additionally, backlighting of HED plasmas with high-energy charged particles has recently provided new insights into magnetic and electric field generation and evolution in contexts relevant to ICF, basic plasma physics and laboratory astrophysics.[5–10]

The solid-state nuclear track detector CR-39[11] has provided the basis for many neutron and charged particle diagnostics[5,12–20] for HED and ICF experiments at both the OMEGA laser facility[21] and the National Ignition Facility (NIF).[22] CR-39, a transparent plastic, detects charged particles with energy on the order of 1–10 MeV with 100% efficiency. High-energy charged particles leave trails of broken molecular bonds in the bulk of the plastic. These damaged regions are etched faster than the bulk plastic by a sodium hydroxide solution, leaving conical pits or 'tracks' with diameters on the scale of microns.[23,24] The diameter of the tracks depends on the energy of the incident particle; calibrations have documented the relationship between diameter and incident energy ("D-vs-E") for protons in the range 1–9 MeV.[25] Environmental effects, such as aging of the plastic[26] and exposure to electrons,[27] high temperatures,[28] UV radiation,[29] and vacuum,[30] have been shown to alter the response of the detector to charged particles, and must be considered in CR-39 applications.

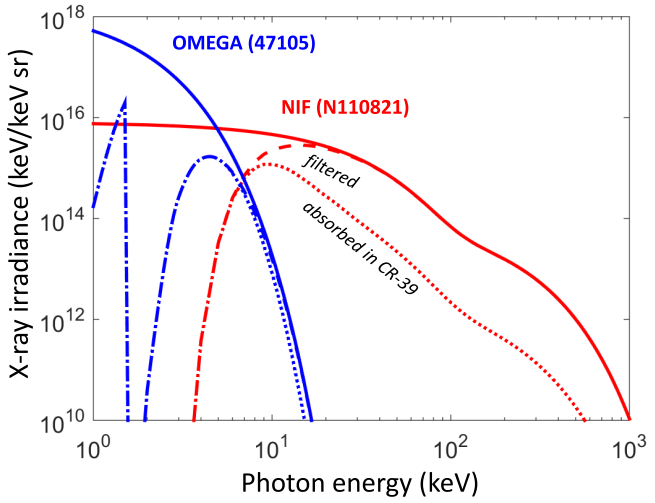

FIG. 1. Measured x-ray spectral irradiance from a direct-drive cryogenic implosion on OMEGA (shot 47105, blue) and from an indirect-drive ignition-surrogate implosion on NIF (shot N110821, red). The calculated spectra after filtering with 25 μm (OMEGA) and 100 μm (NIF) of aluminum, respectively (dashed lines) and the spectra absorbed in CR-39 proton diagnostics (dotted lines; dash-dotted where overlapping dashed) are shown.[31] Estimated absorbed x-ray dose in CR-39 fielded 50 cm from the experiment is 40 and 6 Gy, respectively.

The relative insensitivity of CR-39 to x-ray exposure has contributed to its success in diagnostics at laser plasma facilities, which produce intense x-ray bursts due to laser-plasma interactions. However, recent work has

[a)] Currently at Lawrence Livermore National Laboratory; rinderknecht1@llnl.gov
[b)] Currently at Los Alamos National Laboratory
[c)] Currently at the Laboratory for Laser Energetics

shown that the diameter of tracks produced by alpha particles with energies in the range 1–5.5 MeV are diminished by up to ∼40% with x-ray exposure in the range 0–20 Gy.[32] Doses absorbed by the CR-39 used in charged particle diagnostics on OMEGA and the NIF frequently fall within this range. Figure 1 shows examples of measured x-ray spectra, as well as the calculated filtered spectra and absorption in CR-39 samples, for OMEGA and the NIF. Using the measured x-ray irradiance from a typical directly-driven cryogenic implosion on OMEGA,[33,34] the absorbed dose in a sample of CR-39 fielded 50 cm from the implosion is calculated to vary dramatically over a selection of typical filters: when filtered with 25 μm Al, 50 μm Al or 12.5 μm Ta, the absorbed dose is estimated to be ∼40 Gy, 1.9 Gy, or negligible, respectively. Similarly on the NIF, the measured x-ray irradiance from an indirectly-driven ignition-scale implosion[35] is calculated to deposit ∼6 Gy in the most thinly-filtered (100 μm Al) region of the CR-39 in the Wedge Range Filter (WRF) compact proton spectrometers.[18] The previous study with alpha particles suggests that for doses of this magnitude, the relationship between track diameter and particle energy may be modified, which in turn may impact data analysis.

This work studies the impact of absorbed x-ray dose on the analysis of CR-39-based nuclear diagnostics. A series of controlled experiments was performed to determine how the sensitivity of CR-39 to protons is changed by exposure of the CR-39 to x rays, as described in Section II. The results of these experiments are presented in Section III, and are applied to evaluate how x-ray dose impacts the analysis of data from OMEGA and the NIF in Section IV.

II. EXPERIMENTAL DESIGN

To investigate the impact of x-ray dose on proton track formation in CR-39, samples were irradiated with x rays, exposed to protons with various energies, and then etched in a 6 molar NaOH solution. The TasTrak® CR-39 samples used in the experiment were 1.5 mm thick sheets acquired from TASL,[36] as has been used extensively in charged particle spectrometry and imaging applications in ICF[12,16,17,19,37] and the response of which has been investigated in several related studies.[25,30,38,39] The samples were laser-cut into 5 cm round discs.

The x-ray exposure was performed using two X-RAD thick-target bremsstrahlung x-ray irradiators manufactured by Precision X-ray, Inc.[40] The first instrument, located at the State University of New York at Geneseo (SUNY Geneseo), has a maximum electron beam energy and x ray energy of 160 kV, while the second instrument, located at the Massachusetts Institute of Technology (MIT), has a maximum energy of 225 kV. The spectra produced by these two instruments is shown in Figure 2. The median photon energy absorbed by the CR-39 samples exposed using the 160 kV source was 10 keV, with 50% of the absorbed dose from photons in the range 5.5–11.6 keV; for samples exposed using the 225 kV source, the median absorbed photon energy was

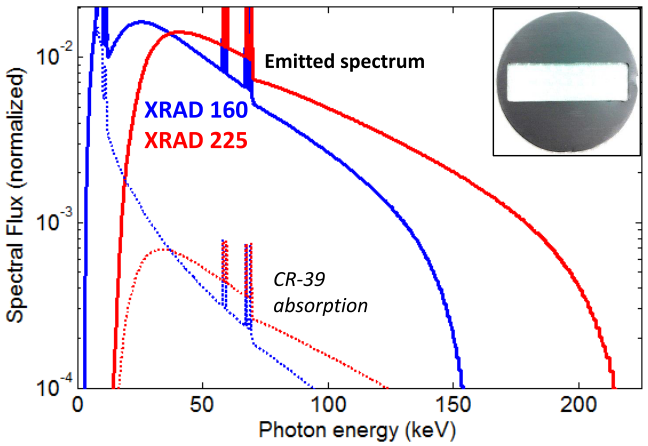

FIG. 2. Area-normalized x-ray spectra (solid) produced by the two X-RAD irradiators used in this study, with a maximum energy of 160 kV (blue) and 225 kV (red), respectively. The 225 kV machine included a 2-mm aluminum filter, blocking x rays below ∼ 20 keV. The spectrum absorbed by the CR-39 for each irradiator (dotted) is calculated based on the mass attenuation coefficients.[31] (inset) A 1 mm thick tantalum mask was used to limit x-ray deposition to a rectangular region of the CR-39. Spectra provided courtesy of Precision X-ray, Inc.[40]

53 keV, with 50% of the absorbed dose from photons in the range 23.5–57.6 keV. The irradiators were absolutely calibrated and set to deliver a desired dose based on an internal dosimeter. The CR-39 samples were exposed to x-ray doses ranging from 2 to 100 Gy before being exposed to protons. A 1 mm thick tantalum mask was used to limit the x-ray dose of the CR-39 samples to a rectangular region, as shown in the inset of Figure 2.

Protons were deposited on the CR-39 samples using two experimental facilities. The Tandem Accelerator at SUNY Geneseo is a National Electrostatics Corporation Model 5SDH 1.7 MV tandem Pelletron accelerator, producing proton beams with energy up to 3.4 MeV. In this experiment, a beam of 3.4 MeV protons with a beam current on the order of 1 nA was produced by the accelerator and injected into the target chamber. The beam passed through a gold scattering foil with a thickness of 0.1 μm positioned at TCC. Protons scatter off the gold nuclei in the foil into the chamber with a cross section described by the Rutherford equation:

$$\frac{\partial\sigma(\theta)}{\partial\Omega} = \left(\frac{Z_t Z_p e^2}{16\pi\epsilon_0 E_b}\right)^2 \sin^{-4}\left(\frac{\theta}{2}\right) \qquad (1)$$

where $\partial\sigma/\partial\Omega$ is the differential cross-section for scattering into an angle θ measured relative to the direction of the beam, $Z_{t,b}$ are the atomic numbers of the target and beam, and E_b is the beam energy.

CR-39 samples were positioned at various angles around the scattering foil for exposure to 3.4 MeV scattered protons. The radial position of the CR-39 samples from the foil was adjusted to partially correct for the angular dependence of the scattering cross-section. Approximately 1.15×10^{-9} of the protons in the beam were also scattered onto a silicon surface barrier detector (SBD) positioned at 90° relative to the beam trajectory,

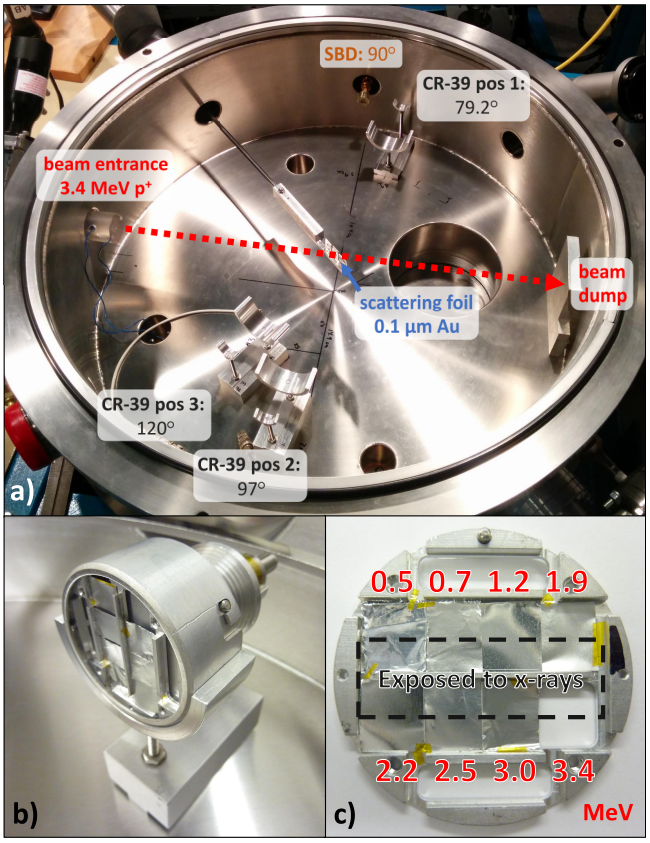

FIG. 3. a) Configuration of the SUNY Geneseo Tandem Accelerator target chamber for proton deposition onto CR-39 samples. The 3.4 MeV proton beam (red dashed) passes through an 0.1 μm gold foil, which Rutherford-scatters protons into the chamber. CR-39 samples (grey) are positioned at 79.2, 97, and 120 degrees to the incident beam. An SBD positioned at 90° to the beam trajectory (orange) is used to infer proton fluence on the CR-39 samples. b) A CR-39 sample pack held in the vacuum chamber. c) Aluminum filters are used to range the 3.4 MeV incident protons down to different energies (red) in eight discrete regions. Each region contains parts both exposed (dashed box) and unexposed to x rays.

which was used to infer the proton fluence on the CR-39 samples fielded in the chamber. The experimental design for these exposures is shown in Figure 3.

The second experimental facility used to deposit protons was the Linear Electrostatic Ion Accelerator (LEIA)[41] at the MIT HED Accelerator Facility for Diagnostic Development. Deuterons were accelerated to 140 keV onto an erbium deuteride target doped with ^{3}He, where a fraction of them underwent one of two fusion reactions:

$$\begin{aligned} D + D &\rightarrow T(1.01\text{ MeV}) + p(3.02\text{ MeV})\ (\sim 50\%), \\ &\rightarrow {}^3He(0.82\text{ MeV}) + n(2.45\text{ MeV})\ (\sim 50\%), \\ D + {}^3He &\rightarrow {}^4He(3.6\text{ MeV}) + p(14.7\text{ MeV}), \end{aligned} \tag{2}$$

where the energy of each resulting fusion product is given. The DD-protons were filtered to produce a range of energies from 1.1–2.9 MeV, and the D^{3}He-protons were filtered to produce a range of energies from 3.5–9.1 MeV.

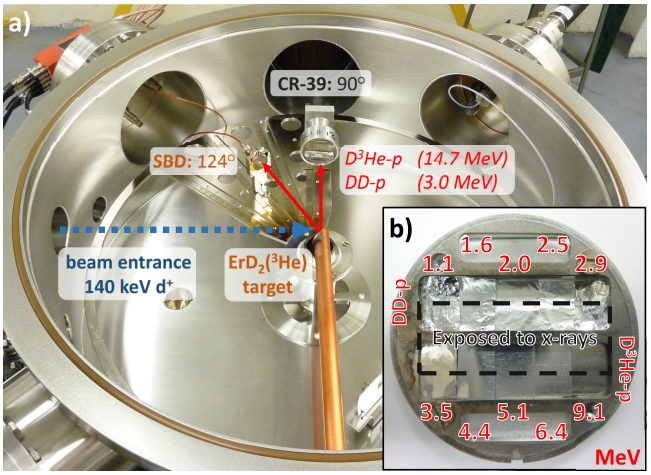

FIG. 4. a) Configuration of the MIT LEIA accelerator target chamber for proton deposition onto CR-39 samples. Beam deuterons (blue dashed) with an energy of 140 keV undergo DD- or D^{3}He-fusion in the ^{3}He-doped ErD_2 target, producing 3.0 or 14.7 MeV protons, respectively. These protons are recorded on CR-39 samples. An SBD (orange) is used to infer proton fluence on the CR-39 samples. b) Aluminum filters are used to range the incident protons down to different energies (red) in ten discrete regions. Each region contains portions both exposed (dashed box) and unexposed to x rays.

The protons were then detected by samples of CR-39 that had been exposed to various x-ray doses, as in the Geneseo experiments. An SBD in the vacuum chamber was used to infer the rate of particle deposition on the CR-39 samples. The experimental layout of these experiments is shown in Figure 4.

After exposure to x rays and protons, the CR-39 samples were etched in 6 molar NaOH solution at 80° C for 3 hours. This procedure follows the standard methodology for CR-39 diagnostics in ICF applications.[12,42]

Following this method, each CR-39 sample provided proton track size data for a range of proton energies at both a given x-ray dose and no x-ray dose.[43] For each combination of x-ray dose and proton energy, three data points were recorded and the results averaged. For protons in the range 0.5–3.4 MeV, two sets of data were obtained using the Geneseo Tandem accelerator and the 160 kV x-ray irradiator, and one dataset was obtained using the MIT accelerator and the 225 kV x-ray irradiator. For protons energies in excess of the 3.4 MeV energy limit of the Geneseo accelerator, all data were recorded using the MIT accelerator and 225 kV x-ray irradiator. This data is presented in Section III A.

Previous experiments using alpha particles demonstrated that the order of exposure of the CR-39 to x rays and charged particle altered the observed effect at the $\sim$ 10% level.[32] Because of these results, in the current study the x-ray dose was always deposited immediately before exposure of the CR-39 to protons.[44] For this reason, the 160 kV x-ray source was used for all experiments on the Geneseo accelerator, and the 225 kV x-ray source was used for all experiments on the MIT accelerator.

In addition, a delay of several weeks between x-ray exposure and etching of the CR-39 was found to result

in a reduction in the observed effect due to x-ray dose, as if the CR-39 had recovered from the x-ray exposure. It was proposed that this recovery was due to (room-temperature) "annealing" of the molecular damage introduced by the x rays, and would therefore be reduced or eliminated by storing the CR-39 at reduced temperatures. All samples in the proton study described above were etched or frozen within a few days of exposure to minimize the recovery effect. Furthermore, a study was performed to test the hypothesis that freezing the CR-39 prevents recovery from an absorbed x-ray dose. A series of CR-39 samples were exposed to 40 Gy using the 225 kV x-ray source, and to various energies of alpha particle. These samples were stored either at room temperature (24.1° C) or in a freezer (-14.1° C) for a period of time ranging from 1 to 30 days prior to etching. The results of this study are shown in Section III B.

III. RESULTS

A. Effect of x-ray dose on proton track diameters in CR-39

The diameters of tracks produced by protons in CR-39 were found to decrease as x-ray dose was increased, as shown in Figure 5. For all proton energies tested, absorption of up to 6 Gy resulted in an approximately linear reduction in the diameter of the resulting track. In the range 6–20 Gy, the rate of reduction with additional x-ray dose decreases, until for 20 Gy and above protons of all energies reach an asymptotic limit. This result is in qualitative agreement with the previous study using alpha particles,[32] suggesting that as in that work, the effect is predominantly caused by a measured change in the etch rate of the bulk CR-39 as a function of x-ray dose, from the initial value of 2.66 μm/hr to an asymptotic value of 1.76 μm/hr at large doses. A fit to the diameter distribution data was performed using the 3-parameter model:

$$D(X) = D(0)\left[1 - (aD(0) + b)\,\mathrm{erf}\left(\frac{X}{X_0}\right)\right], \qquad (3)$$

where $D(0)$ is the track diameter with no x-ray dose and X is the absorbed dose in Gy. This model produced a good fit (R^2=0.995) to all 168 data points with the coefficients $a = -0.0330\pm0.0018\ \mu m^{-1}$, $b = 0.718\pm0.017$, and $X_0 = 8.72\pm0.35$ Gy. The saturation coefficient X_0 is of particular interest: the fit indicates that the saturation point for the track diameter scaling effect is reached for doses of ∼ 9 Gy.

Figure 6 plots the recorded track diameter as a function of proton energy for various x-ray doses. The results of the two different experimental setups are highly consistent with each other. This format clearly shows that the diameter is monotonically reduced as the x-ray dose is increased up to 20 Gy for all incident proton energies. Doses above 20 Gy are not shown, as the response does not continue to change with additional dose above that value.

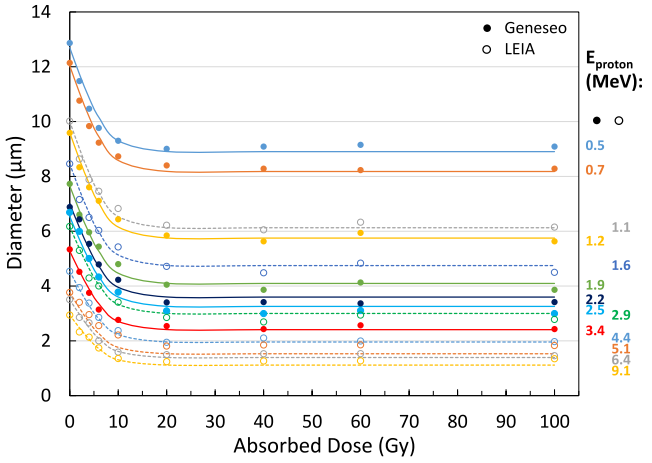

FIG. 5. Measured track diameters produced by protons with various incident energy in CR-39 as a function of absorbed x-ray dose. Data from the Geneseo accelerator (solid points) and from the LEIA accelerator (open points) are shown; some data has been omitted for clarity. For each incident proton energy (colors, indicated in MeV on right) the track diameter decreases monotonically from the nominal value as the x-ray dose is increased to approximately 10 Gy. For x-ray doses in excess of ∼ 20 Gy, the track diameters asymptote to a constant value. A 3-parameter fit defined in Eqn. 3 produces a good fit to all data (lines).

These effects of x-ray exposure on track diameters are of practical significance for CR-39-based charged-particle and neutron diagnostics for at least two reasons. First, if the tracks become too small they are harder to identify and count using automated microscope scanning techniques. Second, analysis of some diagnostic data makes critical use of the absolute diameters of the tracks. This is particularly true for Wedge-Range-Filter proton spectrometers (or WRFs, discussed in Sec. IV C), which make use of a mapping between the diameter of each track and the incident energy of the proton that generated it (the D-vs-E function). That mapping was originally developed by characterizing the sizes of tracks produced by accelerator-generated protons with well-known energies, using the type of CR-39, method of etching, and microscope procedures implemented for WRF data analysis. The resulting D-vs-E curve, shown in Fig. 6 of Ref. [12], was found to be quite repeatable and was used successfully for several years. Eventually the CR-39 manufacturing techniques apparently changed, and it was found that D-vs-E of CR-39 from this supplier was becoming less repeatable and could be quite different between samples even when the handling and processing techniques were held constant.[17,25,30] This problem was eliminated for WRF data by imposing a self-consistency requirement during analysis, which could be satisfied only by choosing the correct D-vs-E function from the one-parameter family of empirically determined functions that are shown in Fig. 7.[17] These functions, specified by the parameter c, were determined through use of a large quantity of WRF calibration data collected on an accelerator,[12,25] and were found to result in extremely consistent inferred proton spectra for all of the CR-39 samples tested. The original

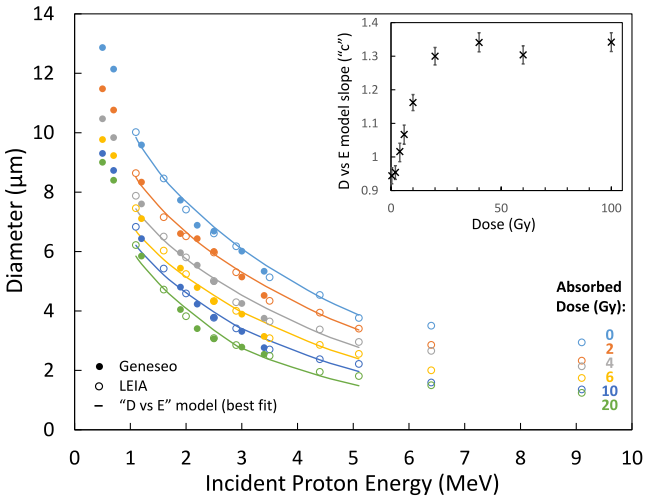

FIG. 6. Measured track diameters produced as a function of proton incident energy in CR-39, for absorbed x-ray dose in the CR-39 from 0 to 20 Gy (points). The track diameter decreases monotonically with x-ray dose (colors, indicated in Gy) for all incident proton energies. A diameter-energy relationship (D-vs-E model) with the shape set by a parameter c (see Fig. 7 and Ref. [17]) was fit to the data in the region 1–5 MeV (lines). (inset) The value of the model shape parameter c that produced the best fit to the data as a function of dose. The shape parameter scales linearly with dose up to a saturating value of ∼20 Gy.

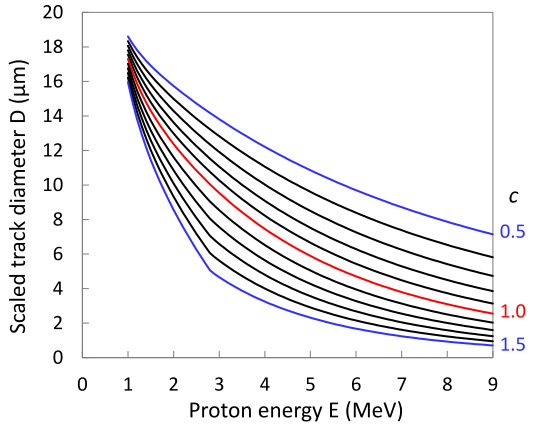

FIG. 7. A family of relationships between track diameter and proton energy (D-vs-E), shown for values of the shape parameter c varying from 0.5 to 1.5 in steps of 0.1 when the maximum proton diameter is 20 μm. These curves are valid in the range $D < 18.5$ μm and $1 < E < 5$ MeV. Before using these curves to relate track data to proton energies, measured proton track diameters must be scaled so the maximum diameter is 20 μm and an appropriate procedure must be found for determining the value of c. These curves are relevant only to the specific CR-39 used and processing developed for CR-39 at MIT, since they are affected by the CR-39 supply, etching procedures, microscope optics, recording cameras, and analysis procedures, and were determined empirically[17] in this context. The mathematical forms of the empirical curves are described in detail elsewhere.[45]

D-vs-E curve[12] is essentially equivalent to the curve for $c = 1.3$ shown in Fig. 7.

This D-vs-E parametrization has been fit to the recorded data, as shown in Fig. 6, to evaluate the effect of x-ray dose on the shape of the response curve. The c value was found to vary strongly with x-ray dose over the region in which track diameters change rapidly with dose. For these data, the slope was found to be shallower ($c \sim 0.95$) when no x-ray dose was applied, but fell off more rapidly as the dose was increased, reaching a limiting value ($c \sim 1.3$) when the impact of additional x-ray dose on the sample was observed to saturate.[46] Since for the purposes of proton diagnosis the response of the CR-39 is characterized primarily by the diameter-energy relationship, the impact of x-ray dose can be interpreted as a local change in the value of the c parameter. As will be discussed in Section IV, this result has practical implications for the analysis used for the WRF diagnostics.

B. Persistence of x-ray effects under various storage conditions

The strength of the diameter reduction effect due to x rays was found to diminish with the time between x-ray deposition and etching of the CR-39. This 'recovery' of the CR-39 with time was studied for CR-39 samples stored at both ambient temperature (24.1° C) and in a freezer (−14.1° C), and the results are shown in Figure 8. CR-39 samples exposed to 40 Gy x-ray dose and alpha particles and then stored at either ambient or freezing temperatures initially produced the same track diameters. However for the ambient samples, the diameter of the produced tracks began to recover within two days of exposure. After 13 days at ambient temperatures, the CR-39 samples had recovered completely: the diameters of tracks produced by etching the CR-39 were the same as if the CR-39 had never been exposed to x rays. In contrast, the frozen samples were not observed to recover: after 28 days of storage, the track diameters after etching were identical to samples exposed and etched on the same day.

Storing the CR-39 at freezing temperatures appears to be sufficient to prevent the recovery of the bulk plastic from the effects of x rays. This finding has several implications for the treatment of CR-39 exposed on ICF facilities, which are discussed in the concluding section.

IV. IMPACT ON CHARGED PARTICLE DIAGNOSTICS

CR-39 is used in a wide range of particle diagnostics on both OMEGA and the NIF. Depending on the physical basis of the diagnostics operation, x-ray dose may impact the interpretation of the data. These diagnostics fall into several categories: magnetic spectrometers, step range filters, wedge-range filters, and imagers. The implications of the above study on each of these categories will be discussed separately. In general, the fact that x-ray dose has been found only to change the diameter of the resulting tracks without altering their apparent flu-

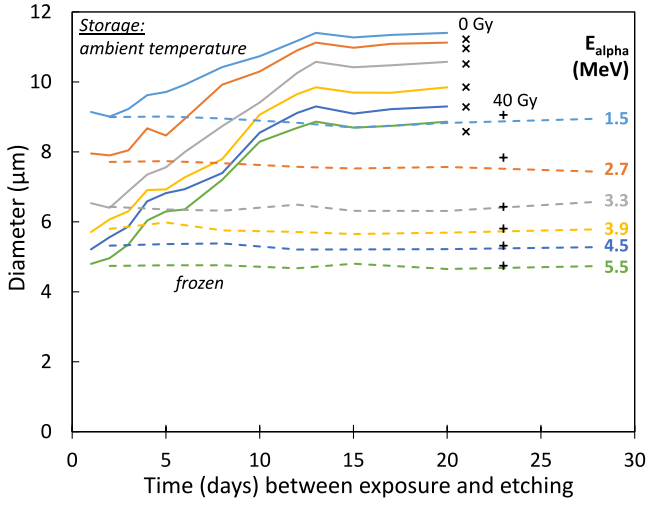

FIG. 8. Measured track diameters produced as a function of time between exposure to 40 Gy x-ray dose and track etching in days, for alpha particles with energy in the range 1.5–5.5 MeV (colors, see legend). CR-39 samples stored at ambient temperature (24.1° C, solid lines) demonstrated complete recovery of track diameters to values equivalent to no x-ray dose (black x) within 13 days. In contrast, samples stored in a freezer (−14.1° C, dashed lines) showed no observable recovery from the previously observed alpha particle track diameters for 40 Gy exposure (black +, see Ref. [32]) over four weeks. Freezer storage is standard operating procedure for CR-39 exposed on OMEGA and the NIF.

ence implies that any experimental x-ray dose will not fundamentally change the operation of most diagnostics. However in a few cases (most notably the WRF diagnostics discussed in Section IV C) the diameter of the tracks is important to the interpretation of the data, and these must be considered in more detail.

A. Magnetic spectrometers

The Charged Particle Spectrometers (CPS1 and CPS2) on OMEGA[12] and the Magnetic Recoil Spectrometers (MRS) on OMEGA and the NIF[3] perform momentum-analysis of incident charged particles by passing them through a fixed magnetic field. The radius of curvature for a charged particle with atomic mass A, atomic charge Z and energy E in the magnet is proportional to $\sqrt{AE}/Z$, such that particles are deflected to different positions on the detectors as a function of their energy. The geometry of the deflecting magnetic system ensures that the detectors do not have direct line-of-sight to the target, shielding them substantially from x rays produced in the experiment. In the analysis of magnetic spectrometer data, the spectrum of incident particles is reconstructed based on the position of measured tracks in the detector plane, not taking the diameter of the tracks into account. Track diameters are used to discriminate between different species of particles: for example, protons and alpha particles with the same energy are deflected to the same position on the detectors. However, the diameters of tracks produced by protons and alphas differ by a factor of 2–3, and x rays have previously been observed to alter the size of alpha particle tracks in a similar way to the proton tracks in this study.[32] Because the diameter shift seems to arise from a change in the CR-39 chemistry, we expect that any charged particle track will be affected in a similar way, and x-ray effects will not interfere with distinguishing between particle species. In summary, any x-ray exposure of the CR-39, uniform or otherwise, will not substantially alter the analysis of magnetic spectrometer data.

B. Step Range Filters (SRF)

The SRF diagnostics are used at the NIF to measure spectra of low energy protons (1–3 MeV).[20] Regions of a single piece of CR-39 are filtered with various thicknesses of tantalum foil in the range 5–55 μm. Incident protons are ranged down by the filters as a function of the filter thickness and detected by the CR-39. The filters also attenuate the x-ray spectrum differently, resulting in a different dose of absorbed x rays and a different diameter-energy relation in each region. The impact of x-ray dose has been observed in some experiments, such as the NIF collisionless shock experiment N141021. Initial processing appeared to show a lower than expected fluence in the region with the thinnest filtering. It was determined that the tracks in the 5 μm Ta region had not been correctly detected by the automated scanning software, as they were smaller than expected based on the track diameters in the other regions. This result was consistent with a substantially larger x-ray dose estimated in this region based on measured x-ray spectra (∼60 Gy) as compared to that estimated for the regions filtered by 10, 15, and 20 μm Ta (8, 2, and 0.4 Gy, respectively). Additional etching revealed a track fluence consistent with the rest of the sample.

The standard mode of analysis for this detector evaluates only the total fluence in each region, using calculations of the number of particles ranged out in the tantalum filters to evaluate the mean initial energy and spectral width of the proton line. As long as the piece has been sufficiently etched and all tracks are observed and counted, this analysis procedure will not be affected by the altered track diameters. Care must be taken in the etching process to ensure that all tracks are sufficiently large to be distinguished from intrinsic noise, but sufficiently small to avoid overlap of tracks in samples with high fluence.[39]

In principle, the diameter-energy relationship may be used to infer more information about the proton spectrum from this data. In the development of such an analysis technique the absorbed dose in each region, which has been shown to vary substantially with the filtering across a single CR-39 sample, must be taken into account.

C. Wedge Range Filter (WRF) proton spectrometers

The WRF proton spectrometers range incident protons through a wedge-shaped aluminum filter prior to recording the protons using CR-39.[12,17] The distribution of proton energy (determined from track diameter) as a function of filter thickness (determined from location on the CR-39) is used to infer the incident proton spectrum. Knowledge of the diameter-energy relationship for the CR-39 is thus essential for an accurate proton spectral measurement using this diagnostic. As mentioned earlier, D-vs-E has been shown to vary between individual pieces of CR-39[17,25] but this variation may be addressed by using an adaptive analysis procedure, in which the unique value of the c parameter is found that results in an inferred proton spectrum being consistent with the spatial distributions of tracks with all measured diameters.[17] The D-vs-E relationship can also be altered by environmental effects,[30] which may be addressed in the same way since these effects generally change the D-vs-E uniformly at all positions on the CR-39. However, any incident x-ray spectrum is differentially filtered by the aluminum wedge and results in a varying absorbed dose as a function of location on the CR-39. As was shown in Section III A, this implies a value of c that also varies as a function of location. The impact of this effect on WRF spectral accuracy is investigated here.

To evaluate the impact of x rays on the inferred spectra, calibration data for a WRF recorded on the MIT accelerator and featuring three proton lines was post-processed to simulate the effect of various x-ray doses.[47] The x-ray absorbed dose as a function of position was calculated using the measured x-ray spectrum from a NIF indirectly-driven D^{3}He-gas filled implosion (N110821),[35] as shown in Figure 9a. Such implosions are demonstrated to be surrogate to cryogenic layered implosions, and WRFs are routinely fielded to measure the spectrum of D^{3}He-protons generated at shock-flash.[48] The overall intensity was scaled to produce a dose at the thinnest WRF position of 5, 10, 20, 50 and 100 Gy; the absorbed doses at each of the three proton lines is shown in Fig. 9b. The diameters of tracks in the calibration data were modified according to the results of Sec. III, using Eqn. 3 with the calculated dose as a function of the track position. The data were then analyzed using the adaptive D-vs-E technique, in which the best-fit value of c was inferred from the highest energy proton line[49] and applied to analyze the entire spectrum. The resulting spectra are shown in Figure 10. The adaptive technique accurately records the spectrum of the high-energy peak regardless of x-ray dose, by accounting for changes in the c parameter. The lower-energy peaks are visibly upshifted in the analyzed spectrum as the dose increases from 0 to 20 Gy, at which point the lowest energy peak reaches saturation-level doses and c is maximally different between the peaks. Because of the saturation of the x-ray effect, additional dose causes c to approach a limiting value everywhere on the piece, and the analysis recovers the original spectrum at $\sim$ 100 Gy. The maximum offset in the inferred energy of the lowest-energy proton peak was an approximately 400 keV 'upshift', while the

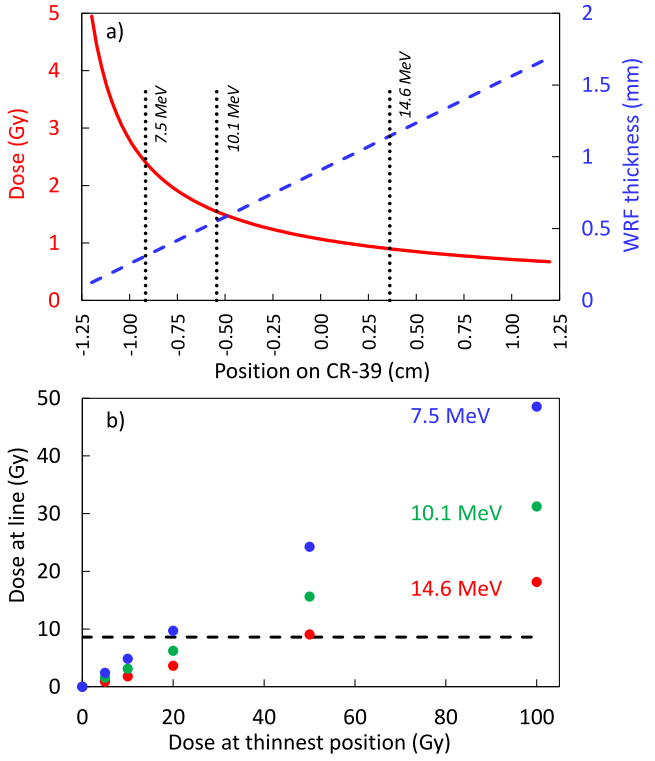

FIG. 9. a) Dose (red) and WRF thickness (blue dashed) as a function of position on the WRF CR-39, calculated based on the x-ray spectrum measured on NIF shot N110821. The positions containing data for three proton calibration energies (black dotted) receive different doses. The CR-39 behind thinnest part of the WRF (at -1.2 cm, thickness $\sim$ 125 μm for this WRF) absorbs $\sim$ 6 Gy with this model. b) Dose absorbed in the regions used to infer the three proton calibration lines at 7.5 (blue), 10.1 (green), and 14.6 MeV (red), as a function of dose absorbed at the thinnest part of the WRF. The lowest-energy proton line reaches x-ray saturation level (X_0 = 8.61 Gy, dashed line) when the dose of the thinnest part of the WRF reaches 20 Gy; all lines reach saturating doses at 100 Gy.

inferred yield in this peak was diminished by a factor of 2 in the most extreme case. The spectral width did not change significantly.

The data are explained well by a change in c with dose as a function of location on the CR-39. Applying the adaptive D-vs-E technique to the lower-energy peaks individually produces different best-fit values for c compared to the high-energy line, as shown in Figure 11. Individually analyzing the low-energy lines correctly reproduces the original spectra for those lines, as was observed for the high-energy line. At high doses, all lines asymptote to the same saturated value of c and the assumption of uniform c is again valid.[50]

An absorbed dose of 6 Gy was calculated for the thinnest region of a WRF fielded on the NIF implosion that produced the x-ray spectrum used in this analysis. Such a spectrum is typical for NIF gas-filled hohlraum implosions, which produce the hottest and most intense x-ray spectra of experiments on which WRFs are typically fielded. (On OMEGA, x-ray spectra are much lower energy than on NIF (see Fig. 1), and doses absorbed by

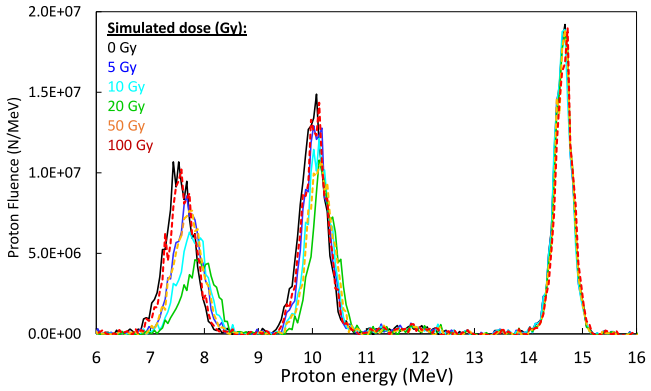

FIG. 10. Proton spectra analyzed from WRF calibration data with simulated x-ray doses of 0 (black), 5 (blue), 10 (cyan), 20 (green), 50 (orange dashed), and 100 (red dashed) Gy at the thinnest part of the WRF. Three proton energy lines at 7.5, 10.1, and 14.6 MeV are deposited on the detector; diameters in the resulting data are adjusted using Eqn. 3 and the dose calculation in Fig. 9 to simulate x-ray dose, and the data is then analyzed using the adaptive D-vs-E method keyed to the 14.6 MeV peak. The lowest energy peak is apparently upshifted by up to 400 keV and its total inferred yield diminished by up to a factor of 2 for simulated doses of 20 Gy.

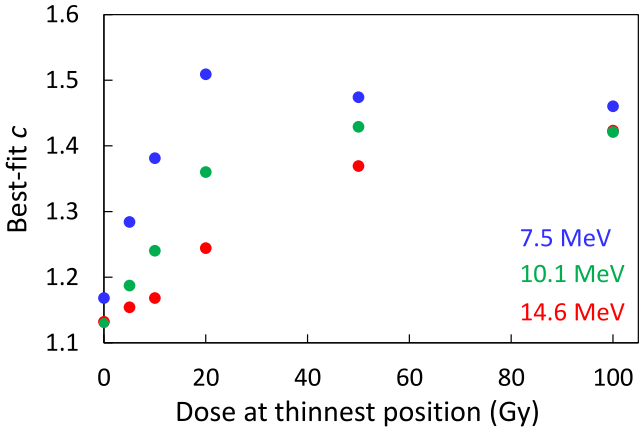

FIG. 11. Best-fit for D-vs-E shape parameter c from analyses with simulated x-ray dose of proton peaks with energy of 7.5 (blue), 10.1 (green), and 14.6 MeV (red). Best-fit c values vary from values of 0.95 with no x-ray dose to 1.3 for saturating x-ray dose in this study. Maximum discrepancy in c occurs at 20 Gy; all lines reach saturating doses at 100 Gy.

the CR-39 in WRF modules is typically negligible.) In practice, most WRF data present a well-defined line of D^3He-protons, for which the adaptive D-vs-E analysis technique accurately accounts for the x-ray dose. In several NIF experiments, protons produced during the compression phase of the implosion, which are ranged down to lower energies, are also detected. Based on this study, application of the c inferred from the shock-flash protons will result in an apparent upshift of the compression-phase proton signal from NIF WRFs of up to ∼150 keV, as well as a reduction in the inferred compression-proton yield of ∼20%. If possible, WRF data with broad spectral distributions should be analyzed using the adaptive D-vs-E technique in each separate region of the proton spectrum. In principle this effect can be taken into account in the analysis of WRF data by the inversion of Eqn. 3 to obtain corrected track diameters as a function of local x-ray dose. This development remains as future work.

D. Charged particle imagers

CR-39 is used as a recording medium for charged-particle backlighting of HED plasmas.[51] In this diagnostic, flat filtering (usually ∼ 10 μm Ta), is interposed between the CR-39 detectors and the experiment. Absorbed x-ray dose will be approximately uniform across the sample, and as such the diameter-energy response to the charged particles will be consistent. Because x-ray dose was found only to shrink tracks and not to make them vanish entirely, the images are not strongly impacted by the effects of x rays so long as the sample is etched long enough for all tracks to be recorded. As long as the energy response curve (c parameter, which was shown to be a function of x-ray dose, see Fig. 6) is consistent across the sample, the energy of tracks in different regions of the sample can be compared in a relative sense by the diameter of the tracks. Accounting for x-ray effects is only important in the event that the absolute energy of the incident particles is required.

CR-39 is also used as a detector for penumbral charged particle imaging of fusion emission in the core of ICF implosions.[52] In this diagnostic a penumbral imaging pinhole, which is typically fabricated from 0.5 mm thick tantalum, is positioned between the source and the CR-39. The relevant data is encoded in the shape of the penumbra in the image plane. Both the charged particle fluence and the x-ray fluence on the CR-39 are shaped by the same penumbral aperture, such that both the x-ray dose and the charged particle fluence vary as a function of radius in the penumbral region. Fortunately, the analysis of this diagnostic depends on apparent particle fluence only, which has been shown not to vary with the x-ray dose. Therefore, the x-ray effects will not alter the penumbral imaging results, as long as care is taken during the etching and scanning process to ensure that all charged particles are counted.

V. CONCLUSIONS

A series of experiments has evaluated the impact of x-ray exposure on the response of CR-39 to protons in the range 0.5–9.1 MeV. Protons are observed to produce smaller tracks in regions exposed to x rays, with the percentage decrease in the track diameter a roughly linear function of x-ray dose up to ∼10 Gy, after which the decrease approaches an asymptotic value. The data were well fit using a three-parameter function accounting for saturation and a linear change in the magnitude of the effect with initial track diameter. Using the established formalism of the track diameter-particle energy relationship, the data can be interpreted as a systematic increase

in the slope of the D-vs-E curve (c) with x-ray dose.

These results indicate that the majority of CR-39-based diagnostics are not significantly affected by x-ray dose, as their analysis depends primarily on the detection of tracks rather than precise knowledge of the D-vs-E relationship. In scenarios where D-vs-E must be known to high precision in the analysis, x-ray effects do play a role. In the most significantly affected diagnostic, the WRF, the analysis procedure in use was found to account accurately for global changes in c. In data with multiple peaks or broad spectra, variation of dose across the sample can introduce systematic shifts in the inferred proton spectra if not correctly accounted for.

The effect of x rays on track formation was found to disappear gradually over the course of approximately two weeks, if the sample is left at room temperature, while the effect was maintained for frozen samples. This result indicates that significant changes in the CR-39 chemistry can occur on the time-scale of days, and confirms the best practice of storing exposed CR-39 samples in the freezer if a significant delay is anticipated between exposure and etching, to preserve the recorded data as accurately as possible.

These results suggest two potential workarounds for x-ray exposure effects, in situations that are sensitive to accurate knowledge of the diameter-energy relationship. Subsequent exposure of the CR-39 sample to saturating doses of x rays ($\gg$20 Gy) just prior to etching may ensure that the D-vs-E relationship is uniform across the sample. Alternatively, sensitive data may be left at room temperature for greater than two weeks to recover from the effect of x rays prior to etching and analysis. Either of these approaches will require development in follow-up studies, but provide a potential means to avoid x-ray effects in sensitive data.

As a comparable reduction in track diameter was observed for both protons and alpha particles, and because the effect appears to be dominated by the bulk etch rate of the CR-39, a similar track diameter reduction with x-ray dose is expected for other ion species as well. Further studies examining the details of track formation for additional ion species will be valuable for continuing to improve CR-39 diagnostics fielded in the extreme environments produced by ICF experiments.

The authors thank the engineering and operations staff at NIF, LLE, and MIT for their support. This work was performed under the auspices of the U.S. Department of Energy by Lawrence Livermore National Laboratory under Contract DE-AC52-07NA27344. This work was done in part for H. Rinderknecht's Ph.D. thesis and was supported in part by the U.S. DoE (DE-FG52-09NA29553), LLNL (B580243), LLE (414090-G), the Fusion Science Center at the University of Rochester (415023-G), and the National Laser Users Facility (DE-NA0000877).

[1] H. Brysk, Plasma Physics **15**, 611 (1973).

[2] C. K. Li, D. G. Hicks, F. H. Séguin, J. A. Frenje, R. D. Petrasso, J. M. Soures, P. B. Radha, V. Y. Glebov, C. Stoeckl, D. R. Harding, J. P. Knauer, R. Kremens, F. J. Marshall, D. D. Meyerhofer, S. Skupsky, S. Roberts, C. Sorce, T. C. Sangster, T. W. Phillips, M. D. Cable, and R. J. Leeper, Physics of Plasmas **7**, 2578 (2000).

[3] J. A. Frenje, D. T. Casey, C. K. Li, J. R. Rygg, F. H. Séguin, R. D. Petrasso, V. Yu Glebov, D. D. Meyerhofer, T. C. Sangster, S. Hatchett, S. Haan, C. Cerjan, O. Landen, M. Moran, P. Song, D. C. Wilson, and R. J. Leeper, Review of Scientific Instruments **79**, 10E502 (2008).

[4] R. Betti, P. Y. Chang, B. K. Spears, K. S. Anderson, J. Edwards, M. Fatenejad, J. D. Lindl, R. L. McCrory, R. Nora, and D. Shvarts, Physics of Plasmas **17**, 058102 (2010).

[5] C. K. Li, F. H. Séguin, J. A. Frenje, J. R. Rygg, R. D. Petrasso, R. P. J. Town, P. A. Amendt, S. P. Hatchett, O. L. Landen, A. J. Mackinnon, P. K. Patel, V. A. Smalyuk, T. C. Sangster, and J. P. Knauer, Physical Review Letters **97**, 135003 (2006).

[6] J. R. Rygg, F. H. Séguin, C. K. Li, J. A. Frenje, M. J.-E. Manuel, R. D. Petrasso, R. Betti, J. A. Delettrez, O. V. Gotchev, J. P. Knauer, D. D. Meyerhofer, F. J. Marshall, C. Stoeckl, and W. Theobald, Science **319**, 1223 (2008).

[7] C. K. Li, F. H. Séguin, J. A. Frenje, M. Rosenberg, R. D. Petrasso, P. A. Amendt, J. A. Koch, O. L. Landen, H. S. Park, H. F. Robey, R. P. J. Town, A. Casner, F. Philippe, R. Betti, J. P. Knauer, D. D. Meyerhofer, C. A. Back, J. D. Kilkenny, and A. Nikroo, Science **327**, 1231 (2010).

[8] M. J.-E. Manuel, C. K. Li, F. H. Séguin, J. Frenje, D. T. Casey, R. D. Petrasso, S. X. Hu, R. Betti, J. D. Hager, D. D. Meyerhofer, and V. A. Smalyuk, Physical Review Letters **108**, 255006 (2012).

[9] M. J. Rosenberg, C. K. Li, W. Fox, A. B. Zylstra, C. Stoeckl, F. H. Séguin, J. A. Frenje, and R. D. Petrasso, Phys. Rev. Lett. **114**, 205004 (2015).

[10] C. M. Huntington, F. Fiuza, J. S. Ross, A. B. Zylstra, R. P. Drake, D. H. Froula, G. Gregori, N. L. Kugland, C. C. Kuranz, M. C. Levy, C. K. Li, J. Meinecke, T. Morita, R. Petrasso, C. Plechaty, B. A. Remington, D. D. Ryutov, Y. Sakawa, A. Spitkovsky, H. Takabe, and H.-S. Park, Nature Physics **11**, 173 (2015).

[11] B. G. Cartwright, E. K. Shirk, and P. B. Price, Nuclear Instruments and Methods **153**, 457 (1978).

[12] F. H. Séguin, J. A. Frenje, C. K. Li, D. G. Hicks, S. Kurebayashi, J. R. Rygg, B. E. Schwartz, R. D. Petrasso, S. Roberts, J. M. Soures, D. D. Meyerhofer, T. C. Sangster, J. P. Knauer, C. Sorce, V. Y. Glebov, C. Stoeckl, T. W. Phillips, R. J. Leeper, K. Fletcher, and S. Padalino, Review of Scientific Instruments **74**, 975 (2003).

[13] J. A. Frenje, C. K. Li, F. H. Séguin, D. G. Hicks, S. Kurebayashi, R. D. Petrasso, S. Roberts, V. Y. Glebov, D. D. Meyerhofer, T. C. Sangster, J. M. Soures, C. Stoeckl, C. Chiritescu, G. J. Schmid, and R. A. Lerche, Review of Scientific Instruments **73**, 2597 (2002).

[14] F. H. Séguin, J. L. DeCiantis, J. A. Frenje, C. K. Li, J. R. Rygg, C. D. Chen, R. D. Petrasso, J. A. Delettrez, S. P. Regan, V. A. Smalyuk, V. Y. Glebov, J. P. Knauer, F. J. Marshall, D. D. Meyerhofer, S. Roberts, T. C. Sangster, C. Stoeckl, K. Mikaelian, H. S. Park, H. F. Robey, and R. E. Tipton, Physics of Plasmas **13**, 082704 (2006).

[15] J. A. Cobble, K. A. Flippo, D. T. Offermann, F. E. Lopez, J. A. Oertel, D. Mastrosimone, S. A. Letzring, and N. Sinenian, Review of Scientific Instruments **82**, 113504 (2011).

[16] D. T. Casey, J. A. Frenje, M. Gatu Johnson, F. H. Séguin, C. K. Li, R. D. Petrasso, V. Y. Glebov, J. Katz, J. Magoon, D. D. Meyerhofer, T. C. Sangster, M. Shoup, J. Ulreich, R. C. Ashabranner, R. M. Bionta, A. C. Carpenter, B. Felker, H. Y. Khater, S. LePape, A. MacKinnon, M. A. McKernan, M. Moran, J. R. Rygg, M. F. Yeoman, R. Zacharias, R. J. Leeper, K. Fletcher, M. Farrell, D. Jasion, J. Kilkenny, and R. Paguio, Review of Scientific Instruments **84**, 043506 (2013), 10.1063/1.4796042.

[17] F. H. Séguin, N. Sinenian, M. Rosenberg, A. Zylstra, M. J.-E. Manuel, H. Sio, C. Waugh, H. G. Rinderknecht, M. G. Johnson, J. Frenje, C. K. Li, R. Petrasso, T. C. Sangster, and S. Roberts, Review of Scientific Instruments **83**, 10D908 (2012).

[18] A. B. Zylstra, J. A. Frenje, F. H. Sguin, M. J. Rosenberg, H. G. Rinderknecht, M. G. Johnson, D. T. Casey, N. Sinenian, M. J.-E. Manuel, C. J. Waugh, H. W. Sio, C. K. Li, R. D. Petrasso, S. Friedrich, K. Knittel, R. Bionta, M. McKernan, D. Callahan, G. W. Collins, E. Dewald, T. Dppner, M. J. Edwards, S. Glenzer, D. G. Hicks, O. L. Landen, R. London, A. Mackinnon, N. Meezan, R. R. Prasad, J. Ralph, M. Richardson, J. R. Rygg, S. Sepke, S. Weber, R. Zacharias,

E. Moses, J. Kilkenny, A. Nikroo, T. C. Sangster, V. Glebov, C. Stoeckl, R. Olson, R. J. Leeper, J. Kline, G. Kyrala, and D. Wilson, Review of Scientific Instruments **83**, 10D901 (2012), http://dx.doi.org/10.1063/1.4729672.

[19]A. B. Zylstra, M. Gatu Johnson, J. A. Frenje, F. H. Séguin, H. G. Rinderknecht, M. J. Rosenberg, H. W. Sio, C. K. Li, R. D. Petrasso, M. McCluskey, D. Mastrosimone, V. Y. Glebov, C. Forrest, C. Stoeckl, and T. C. Sangster, Review of Scientific Instruments **85**, 063502 (2014).

[20]M. J. Rosenberg, A. B. Zylstra, J. A. Frenje, H. G. Rinderknecht, M. Gatu Johnson, C. J. Waugh, F. H. Sguin, H. Sio, N. Sinenian, C. K. Li, R. D. Petrasso, V. Y. Glebov, M. Hohenberger, C. Stoeckl, T. C. Sangster, C. B. Yeamans, S. LePape, A. J. Mackinnon, R. M. Bionta, B. Talison, D. T. Casey, O. L. Landen, M. J. Moran, R. A. Zacharias, J. D. Kilkenny, and A. Nikroo, Review of Scientific Instruments **85**, 103504 (2014), http://dx.doi.org/10.1063/1.4897193.

[21]T. R. Boehly, D. L. Brown, R. S. Craxton, R. L. Keck, J. P. Knauer, J. H. Kelly, T. J. Kessler, S. A. Kumpan, S. J. Loucks, S. A. Letzring, F. J. Marshall, R. L. McCrory, S. F. B. Morse, W. Seka, J. M. Soures, and C. P. Verdon, Optics Communications **133**, 495 (1997).

[22]J. D. Lindl, P. Amendt, R. L. Berger, S. G. Glendinning, S. H. Glenzer, S. W. Haan, R. L. Kauffman, O. L. Landen, and L. J. Suter, Physics of Plasmas **11**, 339 (2004).

[23]G. Somogyi, Nuclear Instruments and Methods **173**, 21 (1980).

[24]H. A. Khan, R. Brandt, N. A. Khan, and K. Jamil, Nuclear Tracks and Radiation Measurements (1982) **7**, 129 (1983).

[25]N. Sinenian, M. J. Rosenberg, M. Manuel, S. C. McDuffee, D. T. Casey, A. B. Zylstra, H. G. Rinderknecht, M. G. Johnson, F. H. Séguin, J. A. Frenje, C. K. Li, and R. D. Petrasso, Review of Scientific Instruments **82**, 103303 (2011).

[26]T. Portwood, D. L. Henshaw, and J. Stejny, International Journal of Radiation Applications and Instrumentation. Part D. Nuclear Tracks and Radiation Measurements **12**, 109 (1986).

[27]J. Charvat and F. Spurny, International Journal of Radiation Applications and Instrumentation. Part D. Nuclear Tracks and Radiation Measurements **14**, 451 (1988).

[28]R. K. Bhatia, R. C. Singh, and H. S. Virk, Nuclear Instruments and Methods in Physics Research Section B: Beam Interactions with Materials and Atoms **46**, 358 (1990).

[29]N. Traynor, C. McLauchlin, K. Dodge, D. Tufano, J. G. McLean, S. J. Padalino, M. Burke, and C. Sangster, *Bulletin of the American Physical Society 59, 5*, (2014).

[30]M. J.-E. Manuel, M. J. Rosenberg, N. Sinenian, H. Rinderknecht, A. B. Zylstra, F. H. Séguin, J. Frenje, C. K. Li, and R. D. Petrasso, Review of Scientific Instruments **82**, 095110 (2011).

[31]J. Hubbell and S. Seltzer, "Tables of X-Ray Mass Attenuation Coefficients and Mass Energy-Absorption Coefficients from 1 keV to 20 MeV for Elements Z = 1 to 92 and 48 Additional Substances of Dosimetric Interest," see `http://www.nist.gov/pml/data/xraycoef/index.cfm` (2013).

[32]J. Rojas-Herrera, H. G. Rinderknecht, A. B. Zylstra, M. Gatu Johnson, D. Orozco, M. J. Rosenberg, H. Sio, F. H. Seguin, J. A. Frenje, C. K. Li, and R. D. Petrasso, Rev. Sci. Instrum. **86**, 033501 (2015), 10.1063/1.4913906.

[33]C. Stoeckl, V. Y. Glebov, D. D. Meyerhofer, W. Seka, B. Yaakobi, R. P. J. Town, and J. D. Zuegel, Review of Scientific Instruments **72**, 1197 (2001).

[34]F. Marshall, J. P. Knauer, T. C. Sangster, J. A. Delettrez, P. W. McKenty, R. Epstein, V. N. Goncharov, and B. Yaakobi, Bulletin of the American Physical Society (2007).

[35]J. W. McDonald, R. L. Kauffman, J. R. Celeste, M. A. Rhodes, F. D. Lee, L. J. Suter, A. P. Lee, J. M. Foster, and G. Slark, Review of Scientific Instruments **75**, 3753 (2004).

[36]Track Analysis Systems Ltd, see `http://www.tasl.co.uk/`.

[37]H. Sio, F. H. Séguin, J. A. Frenje, M. Gatu Johnson, A. B. Zylstra, H. G. Rinderknecht, M. J. Rosenberg, C. K. Li, and R. D. Petrasso, Review of Scientific Instruments **85**, 11E119 (2014).

[38]A. B. Zylstra, H. G. Rinderknecht, N. Sinenian, M. J. Rosenberg, M. Manuel, F. H. Séguin, D. T. Casey, J. A. Frenje, C. K. Li, and R. D. Petrasso, Review of Scientific Instruments **82**, 083301 (2011).

[39]M. J. Rosenberg, F. H. Séguin, C. J. Waugh, H. G. Rinderknecht, D. Orozco, J. A. Frenje, M. G. Johnson, H. Sio, A. B. Zylstra, N. Sinenian, C. K. Li, R. D. Petrasso, V. Y. Glebov, C. Stoeckl, M. Hohenberger, T. C. Sangster, S. LePape, A. J. Mackinnon, R. M. Bionta, O. L. Landen, R. A. Zacharias, Y. Kim, H. W. Herrmann, and J. D. Kilkenny, Review of Scientific Instruments **85**, 043302 (2014).

[40]Precision X-ray, Inc., see `http://www.pxinc.com/`.

[41]N. Sinenian, M. J.-E. Manuel, A. B. Zylstra, M. Rosenberg, C. J. Waugh, H. G. Rinderknecht, D. T. Casey, H. Sio, J. K. Ruszczynski, L. Zhou, M. G. Johnson, J. A. Frenje, F. H. Séguin, C. K. Li, R. D. Petrasso, C. L. Ruiz, and R. J. Leeper, Review of Scientific Instruments **83**, 043502 (2012).

[42]It has been shown that track analysis with 3 hours etch time is equivalent to the standard 5–6 hours, if track diameters are scaled correctly.

[43]Note that this methodology is very similar to that used in the prior alpha particle study described in Ref. [32].

[44]The duration between x-ray exposure and proton deposition was limited by the time required to pump down the accelerator vacuum chambers ($\sim$ 15–30 min).

[45]F. H. Séguin, C. Waugh, B. Lahmann, M. G. Johnson, N. Sinenian, H. Sio, A. Zylstra, D. Casey, H. Rinderknecht, M. Rosenberg, J. Frenje, C. K. Li, R. Petrasso, and R. Bionta, "Compact DD-neutron spectrometer concept for studying ρR, ρR symmetry and yield at Z, the NIF and OMEGA," to be submitted to *Review of Scientific Instruments*.

[46]For typical NIF WRF data, $c \sim 1.2$. Note that this also reflects a significant effect due to vacuum exposure.[53].

[47]The WRF used for this calibration had a minimum and maximum thickness of 125 μm and 1700 μm, respectively. WRFs currently used at the NIF have a smaller minimum ($\sim$ 100 μm) and a larger maximum ($\sim$ 2000 μm), resulting in a larger slope and increased x-ray dose absorbed at the thinnest region. Because the dose and proton energy both scale with the local WRF thickness, this study applies to the NIF WRFs if the nominal dose is calculated for 125 μm thick Al.

[48]A. B. Zylstra, J. A. Frenje, F. H. Séguin, D. G. Hicks, E. L. Dewald, H. F. Robey, J. R. Rygg, N. B. Meezan, M. J. Rosenberg, H. G. Rinderknecht, S. Friedrich, R. Bionta, R. Olson, J. Atherton, M. Barrios, P. Bell, R. Benedetti, L. Berzak Hopkins, R. Betti, D. Bradley, D. Callahan, D. Casey, G. Collins, S. Dixit, T. Döppner, D. Edgell, M. J. Edwards, M. Gatu Johnson, S. Glenn, S. Glenzer, G. Grim, S. Hatchett, O. Jones, S. Khan, J. Kilkenny, J. Kline, J. Knauer, A. Kritcher, G. Kyrala, O. Landen, S. LePape, C. K. Li, J. Lindl, T. Ma, A. Mackinnon, A. Macphee, M. J.-E. Manuel, D. Meyerhofer, J. Moody, E. Moses, S. R. Nagel, A. Nikroo, A. Pak, T. Parham, R. D. Petrasso, R. Prasad, J. Ralph, M. Rosen, J. S. Ross, T. C. Sangster, S. Sepke, N. Sinenian, H. W. Sio, B. Spears, P. Springer, R. Tommasini, R. Town, S. Weber, D. Wilson, and R. Zacharias, Physics of Plasmas **21**, 112701 (2014).

[49]Effectively, the best-fit value for c is that which, when used to infer the proton spectrum, results in the narrowest proton line width.

[50]The discrepancy between c for the three peaks with no applied x-ray dose demonstrates the level of intrinsic variation in this parameter.

[51]C. K. Li, F. H. Séguin, J. A. Frenje, J. R. Rygg, R. D. Petrasso, R. P. J. Town, P. A. Amendt, S. P. Hatchett, O. L. Landen, A. J. Mackinnon, P. K. Patel, V. A. Smalyuk, J. P. Knauer, T. C. Sangster, and C. Stoeckl, Review of Scientific Instruments **77**, 10E725 (2006).

[52]F. H. Séguin, J. L. DeCiantis, J. A. Frenje, S. Kurebayashi, C. K. Li, J. R. Rygg, C. Chen, V. Berube, B. E. Schwartz, R. D. Petrasso, V. A. Smalyuk, F. J. Marshall, J. P. Knauer, J. A. Delettrez, P. W. McKenty, D. D. Meyerhofer, S. Roberts, T. C. Sangster, K. Mikaelian, and H. S. Park, Review of Scientific Instruments **75**, 3520 (2004).

[53]A. Zylstra, *Using fusion-product spectroscopy to study inertial fusion implosions, stopping power, and astrophysical nucleosynthesis at OMEGA and the NIF*, Ph.D. thesis, Massachusetts Institute of Technology (2015).

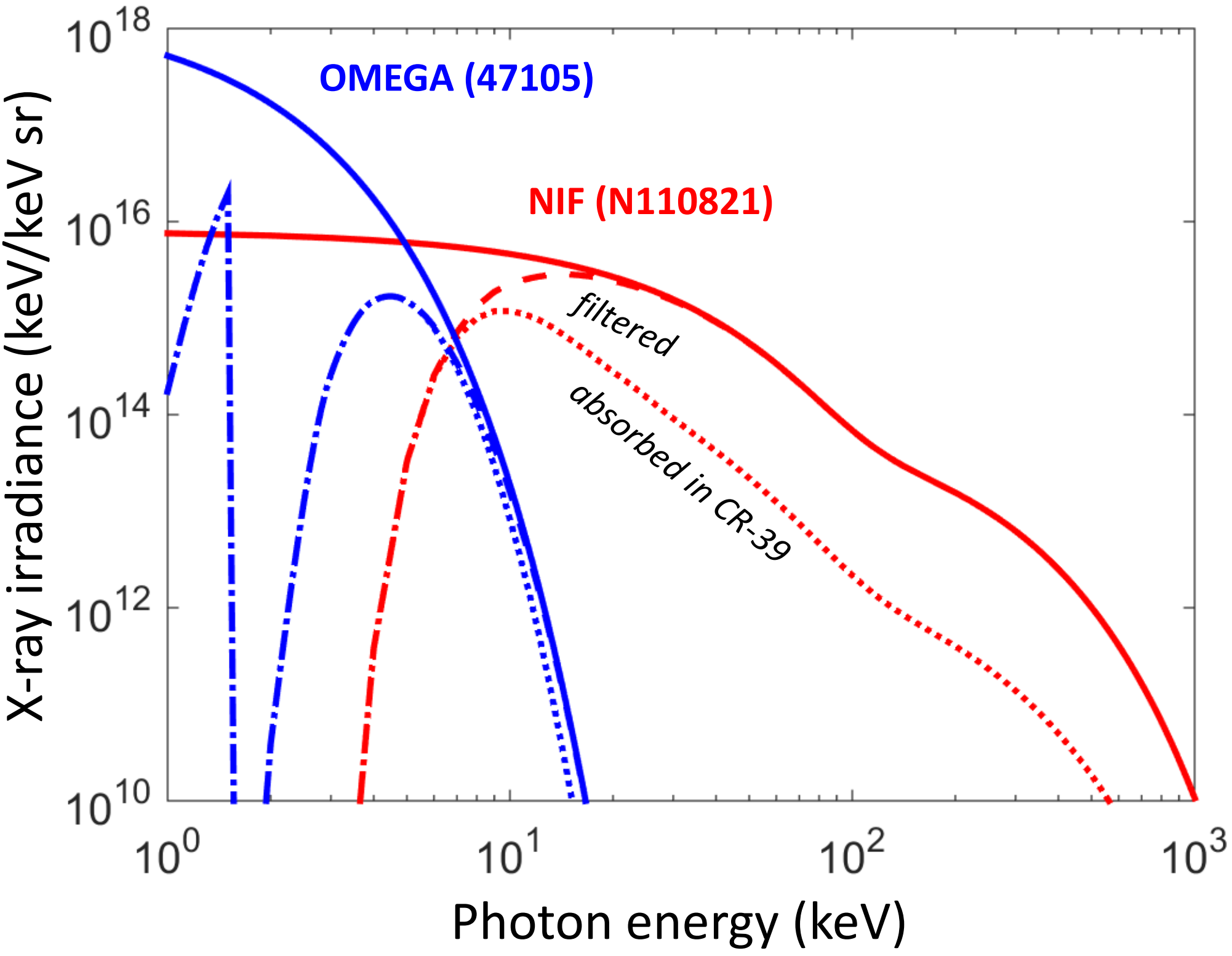
OMEGA (47105)
NIF (N110821)
filtered
absorbed in CR-39
X-ray irradiance (keV/keV sr)
Photon energy (keV)
10^{18}
10^{16}
10^{14}
10^{12}
10^{10}
10^{0}
10^{1}
10^{2}
10^{3}

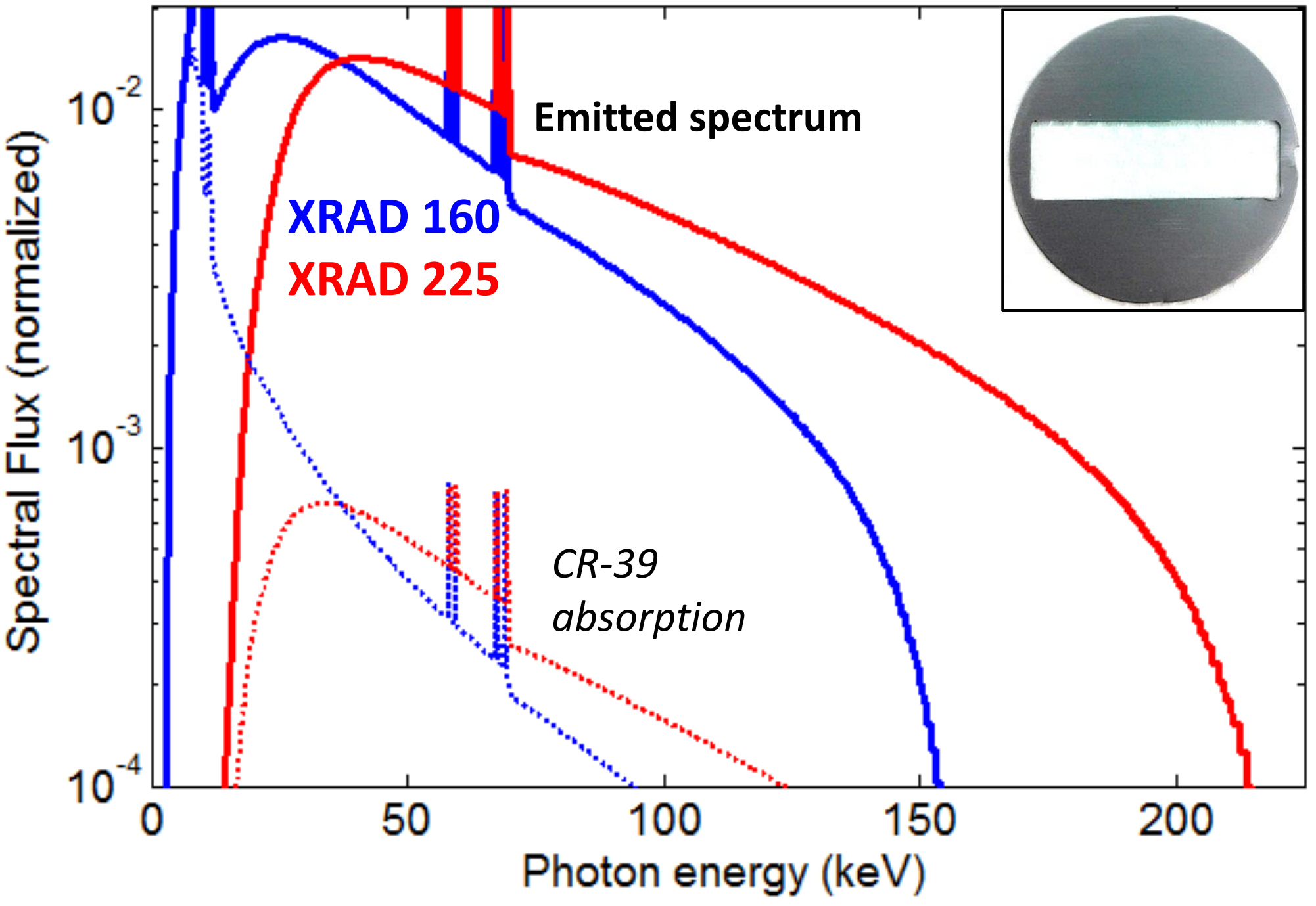
Emitted spectrum
XRAD 160
XRAD 225
CR-39
absorption
Spectral Flux (normalized)
10-2
10-3
10-4
0
50
100
150
200
Photon energy (keV)

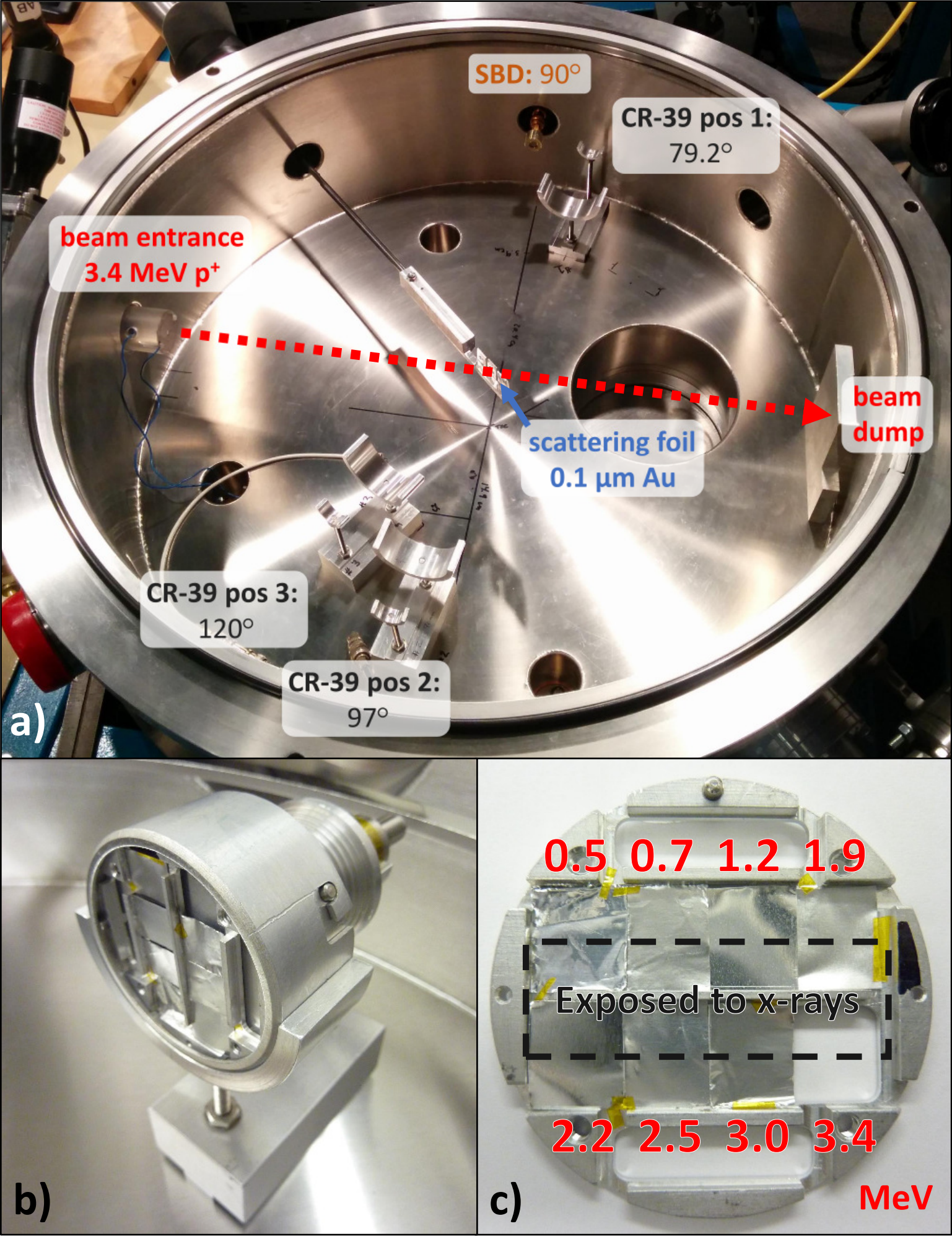
SBD: 90°
CR-39 pos 1:
79.2°
beam entrance
3.4 MeV p+
beam
dump
scattering foil
0.1 µm Au
CR-39 pos 3:
120°
CR-39 pos 2:
97°
a)
b)
0.5 0.7 1.2 1.9
Exposed to x-rays
2.2 2.5 3.0 3.4
MeV
c)

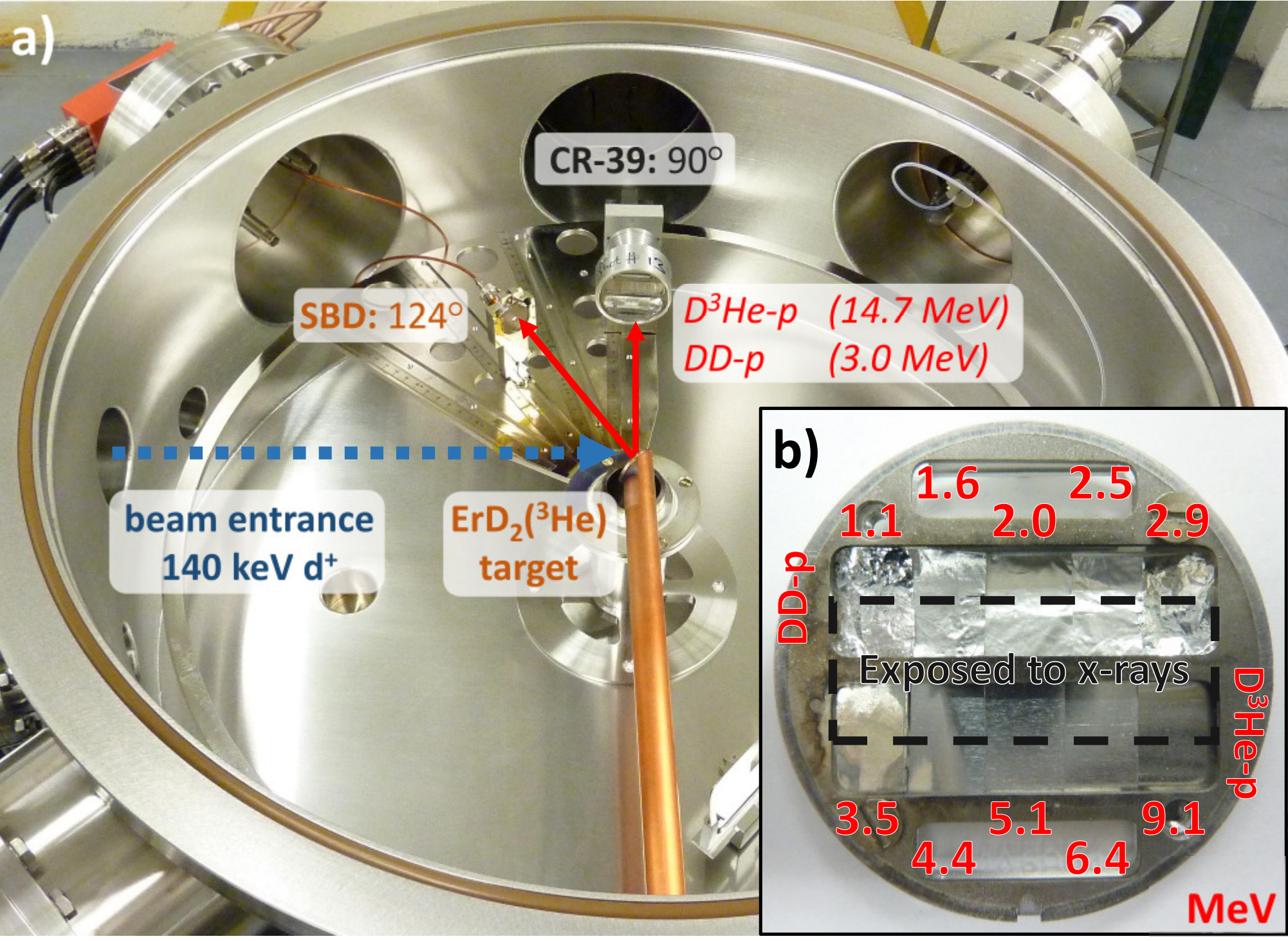
a)
CR-39: 90°
SBD: 124°
D³He-p (14.7 MeV)
DD-p (3.0 MeV)
beam entrance
140 keV d⁺
ErD₂(³He)
target
b)
1.6
2.5
1.1
2.0
2.9
DD-p
Exposed to x-rays
D³He-p
3.5
5.1
9.1
4.4
6.4
MeV

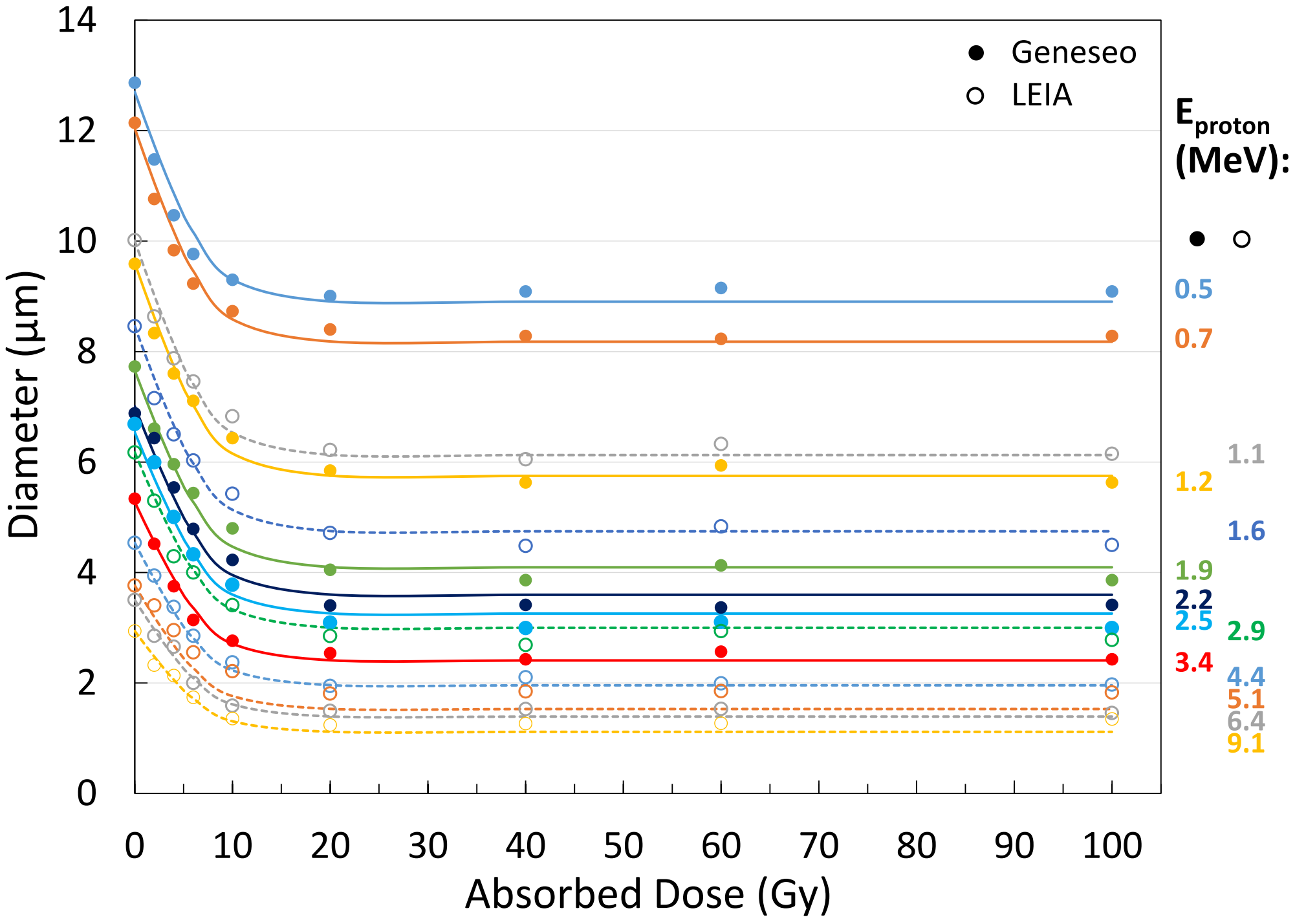
Geneseo
LEIA
E proton (MeV):
0.5
0.7
1.1
1.2
1.6
1.9
2.2
2.5
2.9
3.4
4.4
5.1
6.4
9.1
Diameter (µm)
0
2
4
6
8
10
12
14
0
10
20
30
40
50
60
70
80
90
100
Absorbed Dose (Gy)

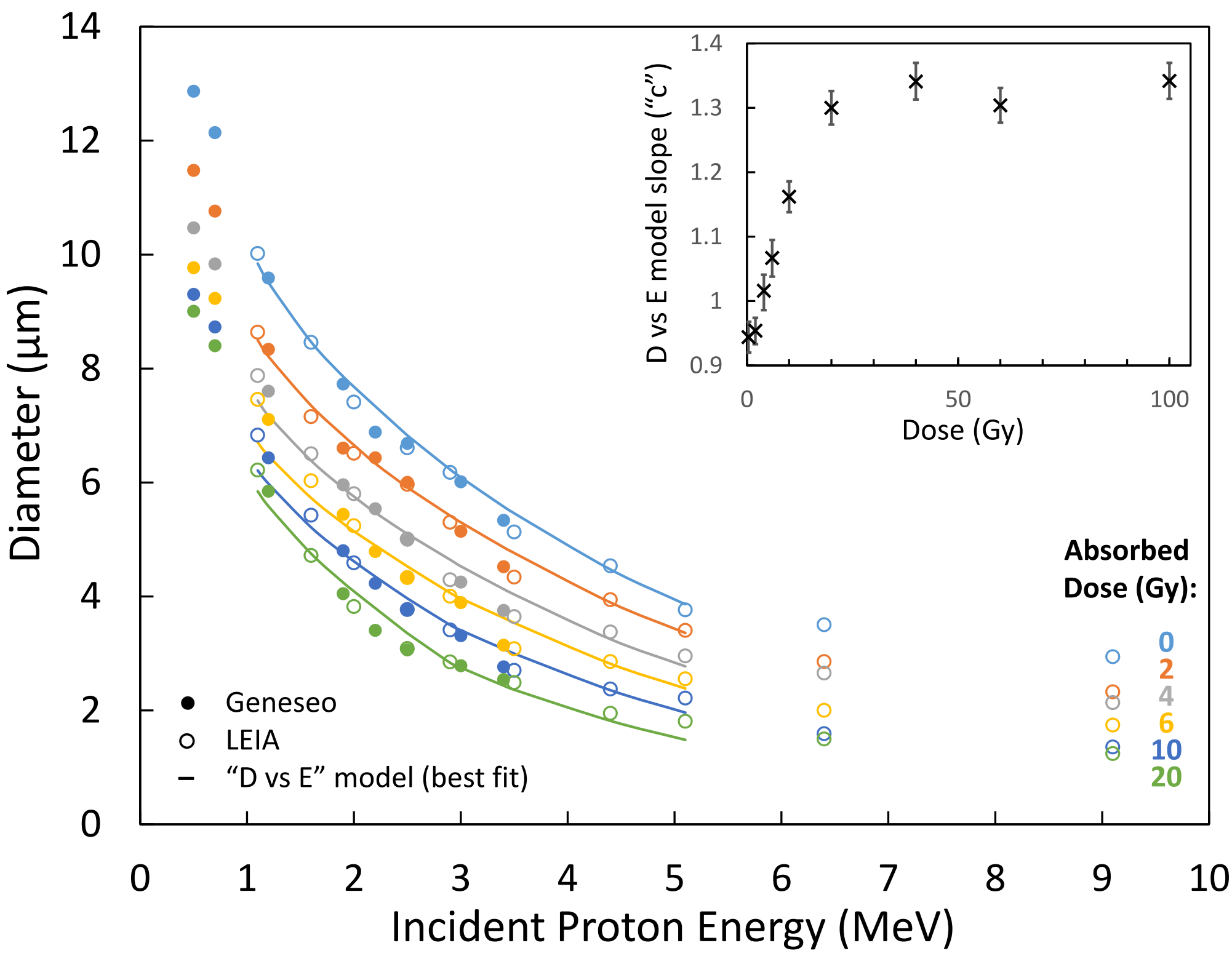
Diameter (µm)
Incident Proton Energy (MeV)
Geneseo
LEIA
"D vs E" model (best fit)
Absorbed Dose (Gy):
0
2
4
6
10
20
D vs E model slope ("c")
Dose (Gy)

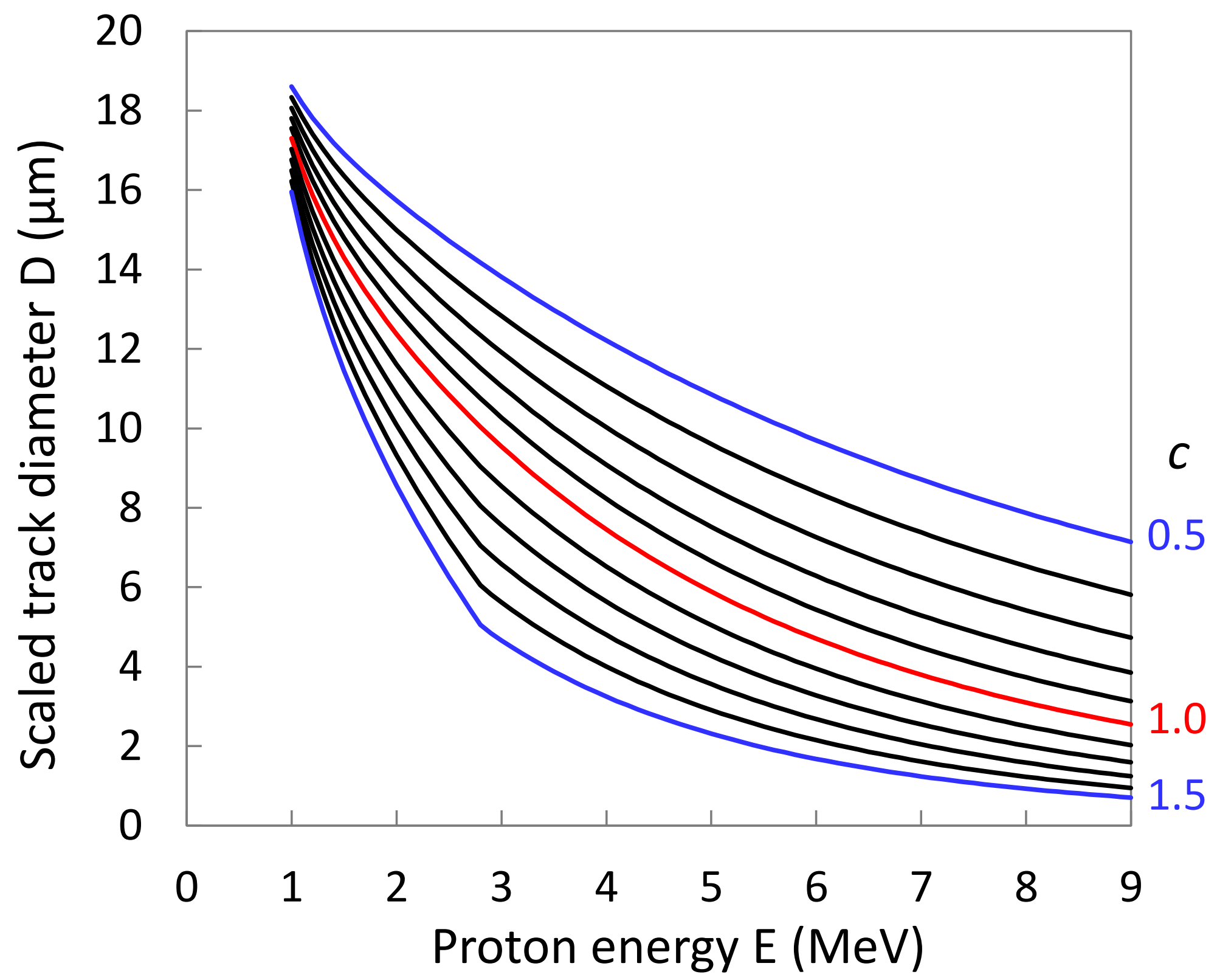
Scaled track diameter D (µm)
20
18
16
14
12
10
8
6
4
2
0
0
1
2
3
4
5
6
7
8
9
Proton energy E (MeV)
c
0.5
1.0
1.5

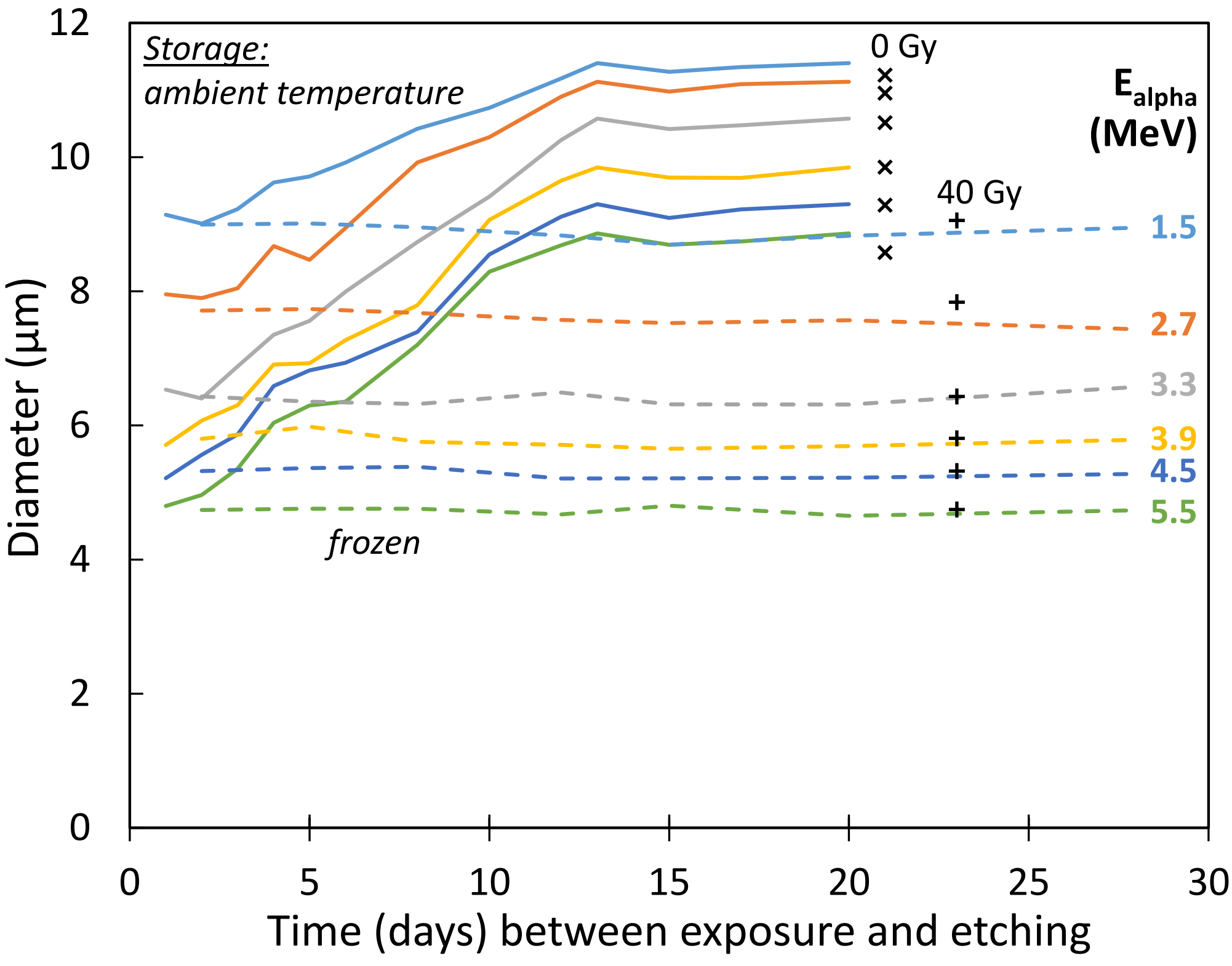
Storage:
ambient temperature
0 Gy
40 Gy
E alpha (MeV)
1.5
2.7
3.3
3.9
4.5
5.5
frozen
Diameter (µm)
Time (days) between exposure and etching
0
2
4
6
8
10
12
0
5
10
15
20
25
30

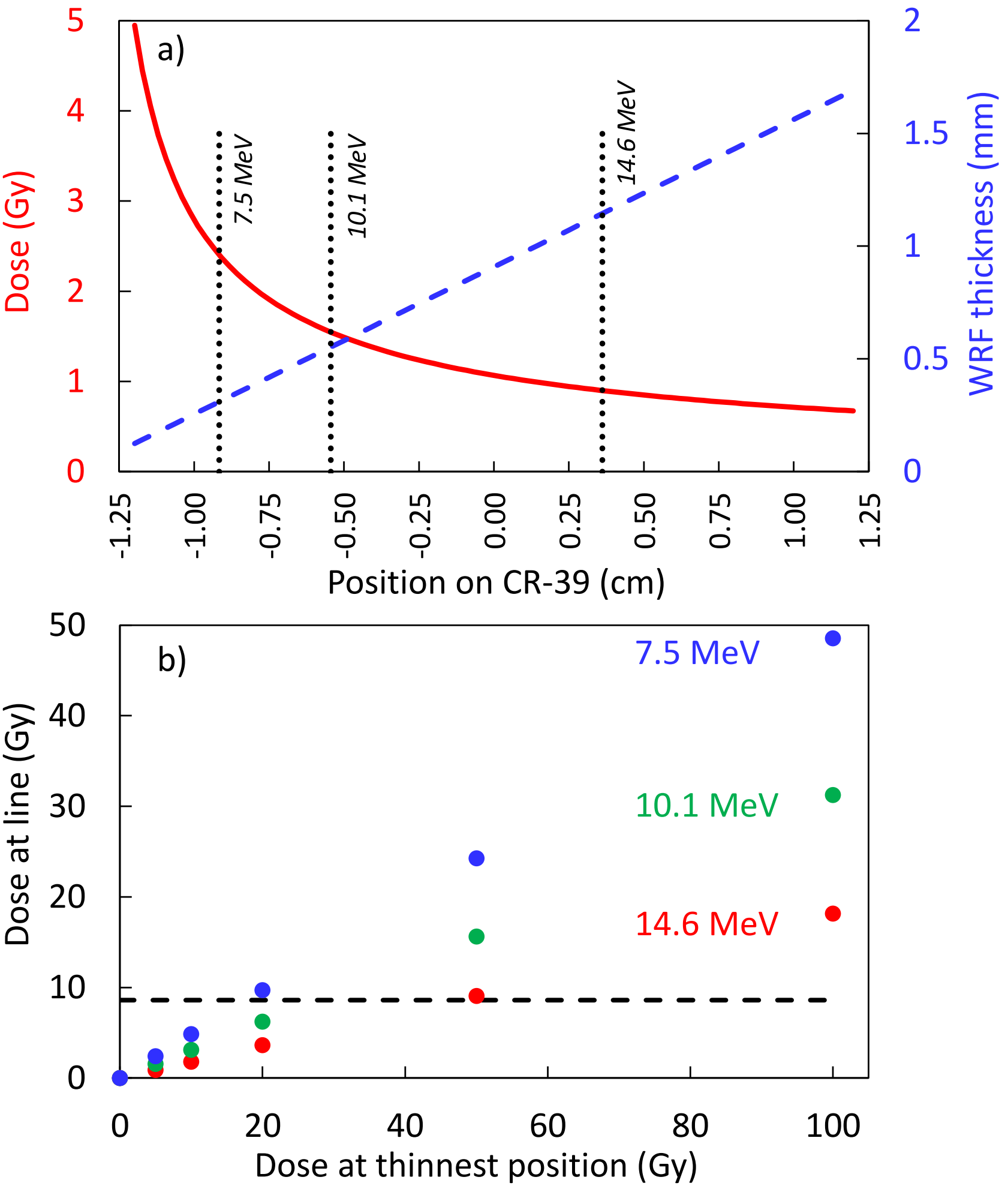
a)
Dose (Gy)
WRF thickness (mm)
7.5 MeV
10.1 MeV
14.6 MeV
Position on CR-39 (cm)
b)
Dose at line (Gy)
7.5 MeV
10.1 MeV
14.6 MeV
Dose at thinnest position (Gy)

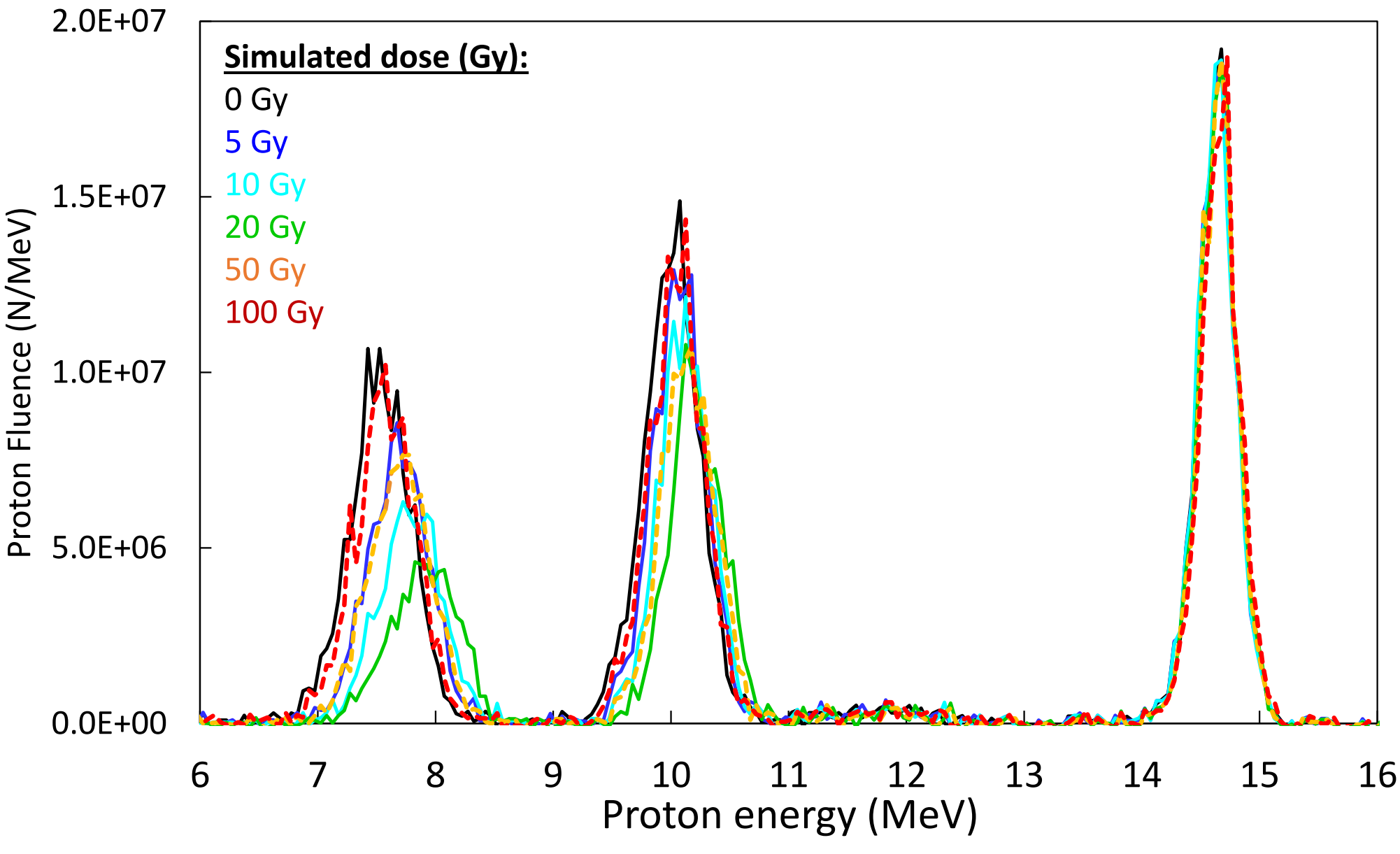
Simulated dose (Gy):
0 Gy
5 Gy
10 Gy
20 Gy
50 Gy
100 Gy
2.0E+07
1.5E+07
1.0E+07
5.0E+06
0.0E+00
Proton Fluence (N/MeV)
6
7
8
9
10
11
12
13
14
15
16
Proton energy (MeV)

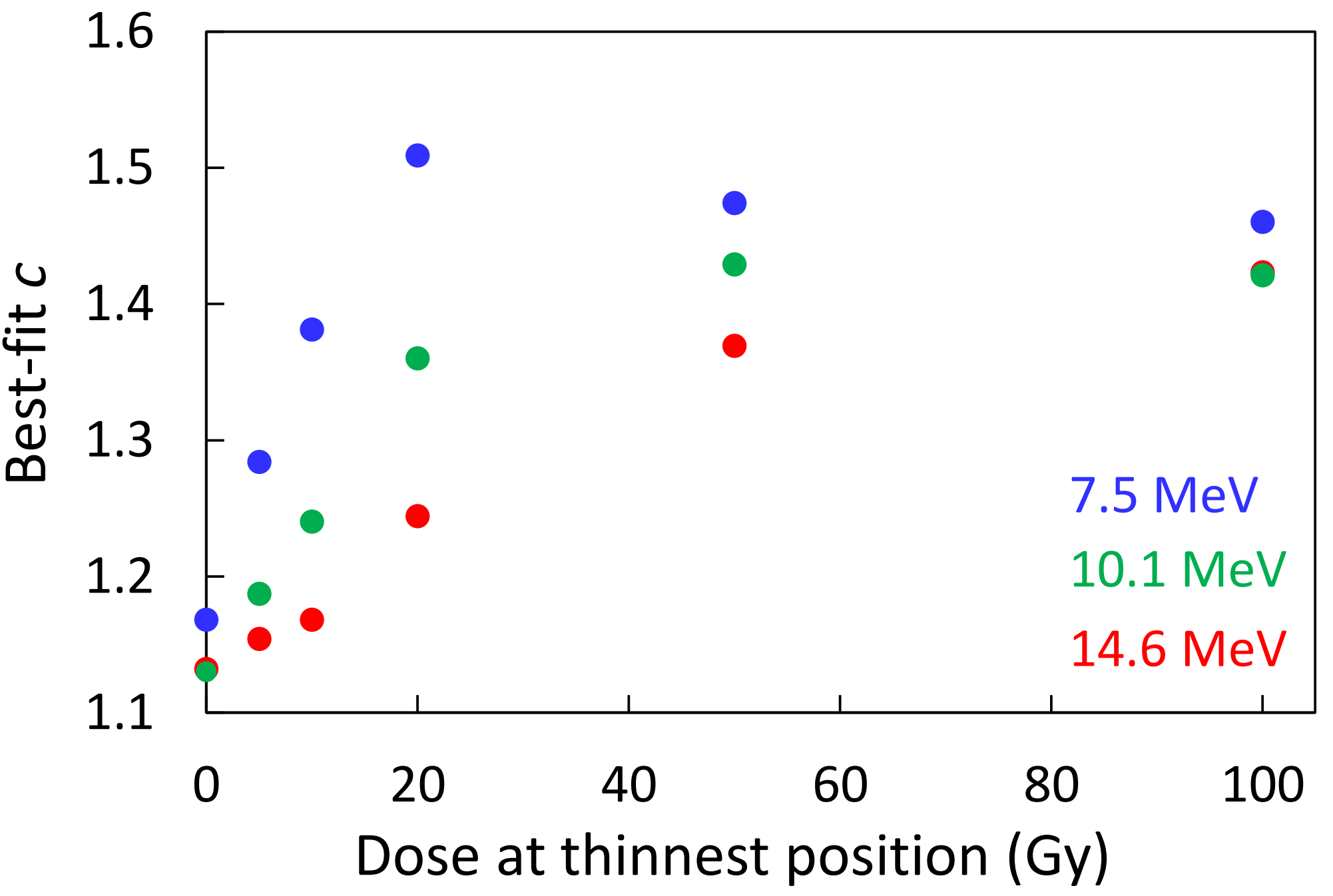
1.6
1.5
1.4
1.3
1.2
1.1
Best-fit c
0
20
40
60
80
100
Dose at thinnest position (Gy)
7.5 MeV
10.1 MeV
14.6 MeV